UNDERSTANDING THE INFLUENCE OF PHYSICAL DYNAMICS ON BIOGEOCHEMICAL FLUXES IN GLOBAL OCEANIC ECOSYSTEMS: AN IMPERATIVE FOR EARTH SYSTEM MODELING AND INTERNATIONAL CLIMATE CHANGE POLICY

By

Alexis Bahl

Department of Environmental Sciences and Policy, Krieger School of Arts and Sciences

---

A capstone submitted in conformity with the requirements

For the degree of: Master of Science

Johns Hopkins University

Baltimore, Maryland

August 2018

Master's Committee

Advisor: Anand Gnanadesikan

Table of Contents

1. Executive Summary

Throughout the geological record, changes in oceans' ecosystem structure have both impacted and been driven by changes in global biogeochemical cycles and carbon storage. The Intergovernmental Panel on Climate Change (IPCC) summarize the risks associated with rising carbon emissions caused by anthropogenic energy demand, but these effects remain to be quantified on multi-millennial timescales. Presently, we are witnessing the effects of increasing global ocean temperatures, and the associated changes on carbonate saturation state, species' adaptive capacity, biogeochemical cycles, and phytoplankton phenology (Parmesan et al., 2003). However, our mechanistic understanding of how marine ecosystems will respond to future variations in climate is still in its infancy, as this requires a multitude of knowledge on the many processes that occur over a wide range of spatial scales and time scales from 1s to 100 years or more. One major uncertainty in projecting future ecosystem states resides in the uncertainties concerning the rate of lateral mixing and its associated effects on biogeochemical cycles. By evaluating the effects when parameterizing six different values of the turbulent diffusion coefficient, A_{redi} (Redi, 1982), we are able to study how the uncertainty in the coefficient propagates to uncertainties regarding changes in saturation state, pH, oxygen, phytoplankton community size structure, and export production. We undergo this study by using a suite of coupled atmosphere-ocean-biosphere models in which the only parameter that is changed is the mixing coefficient. We double and quadruple CO_2 from pre-industrial values to investigate the delayed response on the climate system. Our results show that the impact of employing A_{Redi} as the turbulent diffusion parameter is shown to alter the initial condition of some biological variables, and thus defining the fluxes taking place on a long-term trajectory. Biochemical reactions are not simply driven by changes in mixing, however, instead the impact of defining a diffusion parameter propagates nonlinearly into biological systems. Lastly, our study shows that the anthropogenic increase of carbon dioxide in the atmosphere will result in a change in convection that will ultimately dictate the availability of heat and nutrients to the surface waters, driving changes in calcification which in turn impacts oxygen availability and ocean sequestration. Because the

turbulent diffusion parameter chosen impacts highly nonlinear biogeochemical processes, it governs the effects in a model simulation. Future changes in ocean habitats thus requires further knowledge on the characteristics of ocean overturning to develop a mechanistic understanding for both biogeochemical changes and changes to ventilation at depth. The estimation of this uncertainty provides essential information for assessing climate change risks, impacts, and vulnerabilities, but also for estimating mitigation and adaptation targets for present-day and future international climate change policy agreements.

Keywords: *mesoscale eddies; turbulent mixing; biological pump; carbonate saturation; anthropogenic atmospheric carbon*

2. Plain-English Summary

This study aims to analyze the impacts of increasing CO_2 atmospheric concentrations on global ocean ecosystems caused by human development amongst present-day and estimated future conditions. We particularly study how physical mixing within the oceans water column reacts to increased atmospheric carbon and how the associated changes to physical mixing influences biological, chemical, and geological processes. Each process is extremely important in regulating the global carbon cycle, an exchange between three reservoirs: the ocean, the terrestrial biosphere, and the geosphere that continually acts to erase the gradient in carbon concentration from the surface to the deep, providing the removal of CO_2 from the atmosphere, sequestering it on sub-millennium time scales. The longstanding challenge of analyzing a change in the global carbon cycle is due to studying variables and ecosystem fluxes that vary in space and time. Because ESMs vary in so many different ways, the source of these differences isn't always clear. This study attempts to unravel uncertainties in predicting the fate of future ocean ecosystems by focusing on how a change in a single variable related to physical dynamics within an Earth System Model (ESM) can influence biological, chemical, and geological processes. We find that the particular representation of ocean physics in an ESM nonlinearly impacts changes to biological cycles. Therefore, a better understanding of the uncertainties produced within an ESM is needed when simulating future changes to oceanic ecosystems as the implications have direct impacts on international climate change policy.

3. Introduction

Rapidly rising atmospheric CO_2 concentrations caused by human activity are producing impacts throughout the globe, causing concern as to how the Earth's climate system will respond in the future. If the current rate of carbon emissions persists (2 to 2.5 ppm each year), the planet will experience atmospheric CO_2 concentrations twice the pre-industrial level of 275 ppm_v by the year 2064 (NASA). By the year 2300, atmospheric CO_2 would increase to a peak of more than 2000 ppm_v, given a linear change (Schmittner et al., 2008). Schmittner et al. (2008) found considerable changes when quadrupling CO_2 in an ESM and specifically noted that, even with complete elimination of fossil fuel use by the year 2300, the earth's climate will not result in a return to the pre-anthropogenic state within the next several millennia. Much of this work will be discussed throughout our paper, as the parallels offer considerable insight. The long-term effects of this increase on the oceans include changes to the saturation state, biological production, physical circulation, and sequestration ability.

Shifts in ecosystems associated with climate change have occurred throughout Earth's history. Hain and Sigman (2014) concluded that the impact of warming during the onset of the Bolling-Allerod (B/A) interstadial (near the last stages of the Last Glacial Maximum) resulted in changes to both ocean circulation and biological activity, thereby releasing CO_2 to the atmosphere due to the weakening of the biological pump. The potential consequences of a warming climate and increased greenhouse gas (GHG) emissions on open ocean ecosystems are still unknown due to a number of key uncertainties, among which is the dependence of biotic feedbacks on the physical circulation. For example, because phytoplankton community structure affects the efficiency of carbon export (Dunne et al., 2005; Kwon et al., 2009, Shen et al., 2018), whether communities of species will prove resilient or merely adapt in the future is a question that will also determine the ocean's ability to sequester CO_2. A comprehensive study done by Chust et al. (2014) modeled the possible conditions between 2080 and 2100 under business as usual emissions (Special Repost on Emission Scenarios; Nakicenovic and Swart, 2000), projecting a sea

surface temperature (SST) warming signal of 2.29 ± 0.05°C and an 8.4% decrease in global mixed layer depth, indicating increased global stratification within the water column. As a result, these global simulations suggest primary production will decrease by 9%, zooplankton biomass by 11%, and phytoplankton biomass by 6% (Chust et al., 2014). The analysis between this study and our results will be discussed further as the similar projections of warming on ocean productivity and food web structure contains a parallel that warrants exploration (Chust et al., 2014). Further, the negative amplifications on trophic level biomass through bottom-up control will depend on the timing, rate, and magnitude of change in each stressor, requiring analyses of trophic attenuation on a regional basis and the use of different parameters (Chust et al., 2014; Deppeler and Davidson, 2017). Analysis of the empirical and mechanistic model developed in this study forces us to ask one of the many questions: how does employing physical parameters affect phytoplankton biomass?

In order to answer this question, we must first discuss the tool used for analysis. We conduct our study using an Earth System Model (ESM), a modeling framework most commonly used to integrate the reactions of atmosphere, ocean, land, ice, and biosphere to emulate the current and future states of climate interactions. ESMs allow us to forecast climate change effects by coupling natural ecosystem fluxes with anthropogenic components. Prinn (2011) states that the potential benefits of ESMs are the discovery of new interactions among natural and human climate system components, objective assessment of uncertainty in economic and climate projects, critical and quantitative analysis of policy proposals, and understanding connections to other science and policy issues, such as air pollution. However, ESMs contain a number of uncertainties, a majority of which come from a lack of understanding tracer behavior and having to physically quantify this behavior in an intrinsically coupled system (Prinn, 2011). While scientific consensus and most model projections agree that ocean acidification will amplify under climate change, the response of this amplification on carbonate saturation, primary production, and the physical pump is still being discussed (Hartin et al, 2016). This is because ESMs modify the rate and magnitude of

change depending on both the scenario and the underlying dynamics. The latter can depend sensitively on the values of parameters used to represent specific processes.

Understanding such uncertainties requires in-depth parameter sensitivity studies and uncertainty analyses (Hartin et al, 2016). A particular area of uncertainty relates to the fact that the ocean is turbulent at all scales larger than a few millimeters. The impact of this turbulence on transport mixing at scales smaller than model resolutions is generally represented in terms of a turbulent diffusion coefficient. However, when it comes to the coefficient used to parameterize lateral mixing, examination of the literature reveals significant differences in values estimated from observations, ranging from 70 $m^2 s^{-1}$ in parts of the North Atlantic (NA) to 1,500-35,000 $m^2 s^{-1}$ in the equatorial regions (Gnanadesikan et al., 2018). As a result, models use a range of values for the mixing coefficient thereby producing uncertainties in projection. Because these uncertainties feed directly into present-day politics and government affairs, an examination of their structure and magnitude is necessary to not only enhance our scientific understanding of marine biogeochemical fluxes and physical dynamics, but also to support mitigation and adaptation strategies to lessen climate change risks and impacts (Maslin, 2013).

It is also important to discuss the nutrient supply mechanisms differ regionally by biomes. For example, at 5°S and 5°N, the equatorially-influenced biome experiences upwelling along the equator and rapid horizontal transport out of the upwelling band, generating a high supply of nutrients. On the contrary, just north of these biomes are the pole-ward biomes located in the subtropical gyres defined by a broad band of downwelling velocities. The comparison of these biomes is to shed light on the difficulties involved when parameterizing variables that vary regionally in respect to convection. In areas where surface nutrient concentrations are already zero, this change will not result in reduced nutrient availability, such as high-latitude regions, nor dissolved inorganic concentrations (DIC). This feedback is analogous to warmer waters, which carry a larger degree of change in the mid-latitudes, and the tropics, where thermal stratification limits vertical mixing, decreasing the amount of nutrient supply to the pelagic zone and further limiting phytoplankton growth (Riebesell et al. 2009).

Regional differences also occur due to light limitation. The amount of organic matter photosynthesized in the well-lit layer, commonly known as the euphotic zone (100 m), depends on the amount of sunlight which varies daily and seasonally (Riebesell et al. 2009). If the thickness of the mixed layer is greater than the euphotic zone, which generally only occurs in the wintertime, the phytoplankton organisms will spend a majority of their time in the deeper parts of the ocean (Riebesell et al. 2009). This is because phytoplankton cannot control their vertical distribution in the water column against the overturning motion in the mixed layer. Sweeping them to depths outside of the euphotic zone will generally result in death, as there is not enough light for their growth to exceed respiration (Riebesell et al. 2009). Therefore, models that parameterize might experience an imprecise estimation of phytoplankton populations due to the thickness of the mixed layer employed.

This study aims to quantify how much of our uncertainty in projecting changes in biological and chemical fluxes (e.g. saturation state, pH, oxygen, phytoplankton community size structure, alkalinity, and export production) are due to uncertainties in lateral turbulent mixing. The remainder of this paper is divided into seven sections. Section 4 describes the model used and provides a detailed explanation on how and why we choose to parameterize turbulent diffusion. Section 5 is a full sensitivity study of the employed parameterizations in the mean state and includes discussion on biases and sensitivities. Starting with subsection 5.1., which describes our method of analysis, we focus on a particular parameter, the lateral mixing coefficient A_{Redi} which varies significantly across climate models. Our experimental design involves use of a suite of six coupled atmosphere-ocean-biosphere models in which the A_{Redi} coefficient is the only parameter that is changed. Further, subsection 5.2. discusses the difference between our control models and observations in order to discuss the steady state fields and the model response to the six employed parameterizations. This includes an assessment of the chemical fluxes and bio-physical fluxes in the mean state compared to observations. As we will see, the different models have a similar uptake of heat under increasing CO_2, but produce different responses of circulation, primary productivity, remineralization, oxygen depletion and carbonate saturation depending on the A_{Redi} coefficient used.

Section 6 presents our results. Each of the 7 subsections discusses specific changes when applying parameterization under doubling CO_2 and quadrupling CO_2. We conduct this analysis to investigate the delayed response on the climate system when parameterizing A_{Redi}, and thus determining the linear or nonlinear relationship between physical dynamics and ecosystem response. We finish the paper by discussing our findings in section 7 and the policy implications in subsection 7.1. The results gained by this study are motivated to improving our knowledge of the uncertainties driven by physical dynamic parameters, as well as providing a better understanding of the various biogeochemical fluxes impacted by the parameter employed. Lastly, the efforts produced by this study are done to increase transparency on the strengths and weaknesses of ESMs for developing appropriate climate change policies.

4. Model Description

The work presented here was analyzed with ESM2Mc, a lower resolution version of the fully coupled Earth Systems Model CM2.1, developed at National Oceanic and Atmospheric Administration's (NOAA's) Geophysical Fluid Dynamics Laboratory (ESM2M, Dunne et al., 2012). ESM2Mc simulates atmosphere, land surface, sea ice, and ocean dynamics with full inclusion of oceanic and biogeochemical components using an updated version of the GFDL code, which was prepared in anticipation for the Intergovernmental Panel on Climate Change (IPCC) Fifth Assessment Report. Galbraith et al. (2011) studied the solution produced by the baseline version of the model and stated that although the atmospheric and oceanic grids have been coarsened to decrease computational costs, substantial changes were made to benefit the ocean component to account for subgrid-scale parameterizations. A detailed description of the model can be found in Galbraith et al. (2011).

4.1. Atmospheric Model Configuration

AM2 (Atmospheric Model, version 2) simulates the atmospheric component of the model with a latitudinal resolution of 3° and longitudinal resolution 3.75°, with 24 levels. AM2 employs an M30 grid

by using the finite volume dynamical core studied by Lin (2004), which was implemented in CM2.1 (Delworth et al., 2006). The time steps are increased from from that used in CM2.1 from 0.5 to 1.5 h for tracers, from 6 to 9 min for the dynamical time step, and from 2 to 3 h for the radiative time step. The atmospheric configuration includes an explicit representation of the diurnal cycle of solar radiation, and accounts for aerosols, mixing schemes, and greenhouse gases. The parameter values used are largely identical to those in ESM2M.

4.2. Ocean Module and Bathymetry

The ocean component of ESM2Mc is MOM4p1 (Modular Ocean Model, version p4) (Galbraith et al., 2010), which accounts for explicit physical representation of some equatorial currents using a tripolar grid with the finest latitudinal resolution of 0.6°, though the horizontal dimensions of the ocean grid vary according to latitude (Galbraith et al., 2011). There are 28 vertical levels, nine of which cover the top 100 m, ranging from 10 m resolution at the surface to 506 m in the lowermost layer (Dunne et al., 2005). Tracer advection uses the Sweby MDFL scheme. An ocean-only version of this model, in which surface forcing is a repeated climatological year derived from the Coordinated Ocean Reference Experiment (Griffies et al., 2009). Surface salinities are restored to observations with a 10-day time constant over the top layer, used in Galbraith et al. (2010), in order to calibrate the biological model.

Bathymetry was carefully determined by averaging satellite-derived bathymetry onto the coarser model grid with a smoothing algorithm. To allow for a more realistic representation of bathymetry, the model employs partial bottom cells (Adcroft et al., 1997; Pacanowski and Gnanadesikan, 1998). Where coarse resolution of the topography does not resolve narrow connections, the cross-land mixing scheme by Griffies et al. (2005) is employed, generating less than 2 Sv of total mixing at each location. Finally, vertical mixing is accounted for with a background diffusion coefficient in the ocean, which is, $1 \times 10^{-5} m^2/s$, plus a parameterization of tidally-forced mixing that depends on the local tidal amplitude and bottom roughness (Simmons et al., 2004).

Biogeochemical cycles are accounted for with the use of BLING: a highly parameterized, fully prognostic module that accounts for biogeochemistry with Light, Iron, Nutrients, and Gases (Galbraith et al., 2010). Eight explicit tracers are run in BLING, six of which - dissolved inorganic carbon, alkalinity, micronutrient (nominally Fe), macronutrient (nominally some mix of NO_3 and/or PO_4), dissolved organic material, and oxygen - are prognostic variables with global sources and sinks, meaning that they are advected and diffused like other tracers by the physical environment in the model (Galbraith et al., 2010). Further, the "continuous" character of the model allows for the same equations to be applied at all of the grid cells, eliminating the division between shallow export in the upper boundary layers and remineralization in the deep ocean, which, as stated previously, could otherwise influence fluid dynamics throughout the entire system (Galbraith et al., 2010).

The additional two tracers are "preformed", DIC_pre and PO4_pre, and are set to the modeled values in the mixed layers. While the preformed tracers are advected and diffused in the same way as the prognostic tracers, they have no source of remineralization in the interior, allowing us to break apart changes in biological cycling from changes in circulation. We compute PO_4 remineralization, otherwise denoted as PO4_remin, by subtracting PO4_pre from PO_4, which gives us the amount of phosphate added (and implicitly oxygen consumed) by biological activity. Without simulating the tracer itself, the best method to account for the amount of phosphate that is drawing down oxygen and increasing carbon storage in the ocean. In addition, we have chosen to use particulate carbon as the measure of biomass instead of the more commonly used variable, chlorophyll (Chl), because it reflects cellular energy content and within our model, light saturated photosynthesis is assumed to be proportional to organic carbon concentration. More information can be found in Geider et al. (1997).

Phytoplankton growth rates are computed using the simulated light (which depends on the chlorophyll concentration within the water column), micronutrient, and macronutrient (PO_4 is used as the macronutrient in our study), following the theory of Dunne et al. (2005). The resulting growth rates are then fed into a parametrization fitted to observations to solve for the steady state biomass and associated

uptake rates of iron and nutrient (Galbraith et al., 2010). When run in a fully coupled earth system model, the model produces distributions of chlorophyll and surface macronutrients comparable to those associated with models that run many more explicit tracers (Galbraith et al., 2015). The fraction of nutrient exported as particulate matter depends on the growth rate and light limitations, as described in Galbraith et al. (2010). Organic material sinks with a constant velocity of 16 m/day over the top 80 m, but below 80 m, the sinking velocity increases by 0.05 m/day/m (Galbraith et al., 2010). Theus, the rate of remineralization of organic material depends on the oxygen concentration within the water column, which is important to note and discussed in previous work done by our team (Bahl et al., 2018).

The theory explained above used by Dunne et al. (2005) is based on a two-size class phytoplankton model calibrated against net primary production driven by ammonia and nitrate concentrations. An allometric equation is deployed within the model to separate large and small phytoplankton. The four parameters considered are the remineralization coefficient, the detritus production fractions for small and large phytoplankton, and the detritus remineralization rate (Dunne et al., 2005). Large phytoplankton are classified as providing sinking material, not recycled efficiently, and vary considerably in biomass (Dunne et al., 2005). It is assumed that silicon and calcium carbonate production ($CaCO_3^-$) is primarily done through diatoms and coccolithophorids, which are classified as "large" (Dunne et al., 2005). "Small" phytoplankton (*Prochlorococcus, Synechoccus,* and a portion of the picoeukaryotes community) are made up of nanoplankton (nominally 2-5 μm) and picoplankton (nominally <2 μm) (Dunne et al., 2005). Small phytoplankton are described as being efficiently recycled and vary little in biomass (Dunne et al., 2005). Therefore, it is important to note that the difference between big and small is not only related to the size of the phytoplankton species, but also in their total production, including grazing and export. However, partitioning phytoplankton into two classes requires that each have only a single loss term, which prohibits the incorporation of an explicit separation between grazing, mortality, and aggregation in terms of phytoplankton loss. For more detail, please refer to Dunne et al. (2005).

Lastly, BLING's ability to comparably mimic more complex biogeochemical codes such as TOPAZ, a module that runs 26 explicit tracers (Galbraith et al., 2015), makes it a more viable, less costly biogeochemical module that can be embedded within an OGCM to perform parameter sensitivity studies. Using BLING allows us to separate short-term processes associated with biological cycling (with time scales of order days) from longer-term impacts associated with lateral transport (with time scales of order weeks to months). It is an extremely important component when analyzing ESM2Mc, as the model on its own does not resolve mesoscale eddies. How we will parameterize will be discussed in the next section. Lastly, the use of BLING in this study allows us to estimate the uptake of anthropogenic carbon and the impact of global warming on the biological pump and thus carbon storage; adding to the discussion on the capabilities of different modules and models.

4.3. Sea-Ice Model

Sea ice is accounted for within MOMp41 (as previously stated) by the Sea Ice Simulator (SIS) which contains five thickness classes, and allows for "real" freshwater fluxes and a dynamic-thermodynamic sea ice module (Galbraith et al., 2010). Therefore, the impact of changes in ice cover, sea ice transport and and sea ice melt is available to analyze throughout the study.

4.4. Turbulent Mixing Parameterizations

Turbulent flow is defined within fluid dynamics as being made up of many circular currents of water, called eddies (vortices), which vary in size and strength and emerge from strong horizontal (or lateral) shear produced by wind, currents, and/or topography (Dartmouth). That turbulent kinetic energy is constantly transferred from one eddy to the next within the turbulent flow, which explains its chaotic nature in terms of both pressure and flow velocity. The size of the eddies, which will be referred to as length scales throughout this study, range in size from centimeters to hundreds of kilometers, depending on the mean kinetic energy dissipation rate and eddy viscosity (Pradal & Gnanadesikan, 2014). We choose to focus on mesoscale eddies (typically scaling less than 100 km) because they are an important

mechanism for transferring heat, salinity, and nutrients laterally. It is important to note that simulating these eddies requires the use of a model horizontal resolution of ~ 1/10 of a degree (Pradal & Gnanadesikan, 2014). Due to the low horizontal resolution of ESM2Mc, processes associated with mesoscale eddies occur at sub-grid scales and must be parameterized (Pradal & Gnanadesikan, 2014).

Our discussion of parameterization is focused on the Redi Scheme, A_{Redi}, which determines the diffusion of tracers along isopycnals (neutral surfaces) by means of a diffusion operator that is oriented along the isopycnals, using a Fickian diffusion approximation (Redi,1982; Gnanadesikan et al., 2015). Such that the flux of tracer concentration C is given by:

$$F_X^C = -A_{Redi} \frac{\partial C}{\partial x}$$

The flux of concentration tracer C is the amount of substance per volume and for didactic purposes, the equation assumes movement in a steady state (i.e. from an area of high concentration to low concentration) across the x-axis. A_{Redi} serves as our diffusion coefficiennt, which obeys the relationship of the Fickian diffusion process. Finally, the tracer rests on the isopycnal, allowing us to estimate the position, x, which is taken along the length of the isopycnal. Full information can be read at *Concepts, Definitions, and the Diffusion Coefficient*.

Constraining A_{Redi} is important, particularly in frontal convergence regions where energetic mesoscale eddies produce high turbulent mixing (Gnanadesikan et al., 2018). This is because A_{Redi} diffuses tracers along steeply-sloping density surfaces (Sijp et al. 2006; Galbraith et al. 2011). The transport of the tracer goes from high to low concentrations and is proportional to the size of the tracer gradient, which is particularly large in such regions. Thus, parameterizing A_{Redi} carries considerable impact on the exchange between surface and interior waters, which can affect transport of heat and salt (Pradal & Gnanadesikan, 2014) and the rate at which the ocean takes in atmospheric carbon (Gnanadesikan et al., 2015).

In addition to mixing along isopycnal surfaces, one impact of eddies is to flatten tilting isopycnals. This is represented by the Gent-McWilliams scheme (Gent & McWilliams, 1990; Gent et al., 1995) which adiabatically rearranges tracers along isopycnals through an eddy induced velocity. This is determined by the diffusive coefficient, $A_{GM,}$ and the slope of the isopycnal surface, S_x, producing advective, or transport diffusion, flux within geostrophic eddies (Pradal & Gnanadesikan, 2014). The slope is capped at 0.01 to prevent unrealistic velocities near mixed layers where slopes can become infinite (Gent & McWilliams, 1990). Therefore, the flux in the x-direction is estimated by:

$$F_X^C = -C \times A_{GM} \frac{\partial S_x}{\partial z}$$

Further, A_{GM} is sometimes described as a "thickness diffusivity" which homogenizing the spacing between isopycnals is meant to account for the advective effect of the turbulent lateral mixing (Eden et al., 2008). In most current climate models, A_{GM} varies spatially depending on the gradient of the vertical shear over some depth range. In ESM2M A_{GM} is proportional to the shear between 100 m – 2,000 m multiplied by the square of some length scale with a default minimum and maximum imposed at 200 m^2 s^{-1} and 1400 m^2 s^{-1} respectively (Thomas et al., 2017). Gnanadesikan et al. (2018) found that if the associated length scales are scaled to the width of the baroclinic zone the results produce distributions with high values where isopycnals are steep (e.g. in boundary currents) and generate low values where isopycnals are flat, resulting in severely low values in the tropics and the central gyres.

For full understanding, the large-scale overturning circulation in the real ocean is associated with regions of deep convection that allow for significant inflow and sinking at the top of the water column, and an outflow of dense water that propagates towards the bottom, which can then pour over into lighter surroundings areas (Sijp et al., 2006). Therefore, if eddy advection is not parametrized, ESMs will generally overestimate the extent and depth of convection in high-latitude areas that transform water-mass

properties due to determining overturning diagnostically, thus representing sub-grid scale turbulent mixing of tracer properties by way of horizontal diffusivity is extremely important (Sijp et al., 2006). With the consideration that employing values larger than A_{GM} = 2,000 m^2 s^{-1} tends to shut off deep convection and also returns Southern Ocean Ekman fluxes at too light a density resulting in too little light water being supplied to the pycnocline (Gnanadesikan et al., 2018).

In earlier studies, A_{GM} and A_{Redi} were set equal to each other and referred to as the "neutral diffusion" coefficient because theories proposed that the proportional frequency was to be set equal to the baroclinic growth rate, and thus approximating the "thickness" growth rate as proportional to the isopycnal slope (Griffies, 1998). We will refer to this term as the "turbulent diffusion" coefficient. Further, it should be recognized, however, that the two coefficients parameterize different processes and subsequent experience has found that it is necessary to match the two variables for any convective parameterization (Gent et al., 1995). The GM scheme assumes a vertical transport of momentum, while A_{Redi} parametrizes the lateral stirring via diffusion of passive tracers (Gent et al., 1995). Sijp et al. (2006) studied the sensitivity of the North Atlantic Deep Water (NADW) shutdown based on the choice of mixing scheme in Ocean General Circulation Models (OGCMs) and found that models employing the turbulent diffusion coefficient, A_{Redi}, simulates a significant increase in NADW stability compared to models that just run A_{GM}. ESMs that fail to employ A_{Redi} or A_{GM} see unrealistic convection in the water column, causing tracers and water mixing properties to disperse throughout the water column. This not only risks dampening surface fluxes, but tracers that exist along isopycnals, such as oxygen, can be subjugated to a convection depth. This is defined as the maximum depth attained by overturning of gravitationally unstable waters originating at the surface, simulating low values that are otherwise inaccessible (Sijp et al., 2006). This impact can result in different, unrealistic biogeochemical feedbacks in an ESM. Thus, the impact of perturbations to a model, such as freshwater fluxes (FW) or doubling CO_2, is dependent on the mixing schemes employed. Suppressing convection will make the models under-respond to changes in buoyancy, as the impact will likely result in a permanently non-convective state (Thomas et al., 2017).

5. Sensitivity Study of Biogeochemical Cycling to Mixing Coefficient

5.1. Experimental Design

Our study begins by implementing six fields of A_{Redi}, four of which are constant in space and time, denoted as: AREDI400, AREDI800, AREDI1200, and AREDI2400, with the number denoting the value of the coefficient in $m^2 s^{-1}$. AREDI800 is the control case. The remaining two cases, denoted ABER2D and ABERZONAL, vary in space but not in time. ABER2D uses a field derived by Abernathey and Marshall (2013) using velocities derived from altimetric measurements to advect tracers and invert a diffusion coefficient. A key difference between the resulting distribution and the distribution of A_{GM} is that this parameterization produces very large values of mixing coefficient near, but not in, the center of the boundary currents. This is because the relevant length scales for mixing are not (as has been argued for A_{GM}) the width of the baroclinic zone but, rather, the spatial scale over which propagating eddies exchange fluid. When eddies pass through a region rapidly (as they do in boundary currents), water has little time to feel the eddy and is not moved very far. This explains studies such as that of Cole et al. (2015), which found that the lower values of mixing lengths were found in the boundary currents and the highest values of A_{Redi} were found near but not in the frontal regions.

ABERZONAL uses a zonally-averaged version of this coefficient. More information on the description of these simulations can be found in Gnanadesikan et al. (2015) and Pradal and Gnanadesikan (2014). Increasing A_{Redi} from 400 to 2400 $m^2 s^{-1}$ has been shown to produce a strong warming in the northwest Pacific by moving salt into high-latitude pycnoclines, destabilizing these regions, allowing for deep convection, and thus warming the region (Pradal and Gnanadesikan, 2014). In contrast, the effects of increasing A_{REDI} in the Southern Ocean and subtropics results in sea ice drop from 18.0 Mkm^2 to ~10 Mkm^2, simulating much cooler waters compared to the Northern latitudes.

The model was initialized with ocean data from the World Ocean Atlas 2001 (http://www.nodc.noaa.gov/OC5/WOA01/pr_woa01.html) and run with constant 1860 radiative

conditions. The control simulation with a diffusion coefficient, 800 $m^2 s^{-1}$, was then spun up for 1500 years with aerosols and greenhouse gases fixed at pre-industrial values, which will be referred to as the 1860 control run. At year 1500, the lateral diffusion coefficients were changed and all six cases were allowed to run for an additional 500 years with fixed greenhouse gasses (Gnanadesikan et al., 2015). Once the model hit year 1860 (360 years into the control), we perform an additional two perturbations. First, we double CO_2 concentration from pre-industrial (286 ppm_v) for 140 years, setting the value to 572 ppmv. Second, we keep all conditions the same except for quadrupling CO_2 concentration values from pre-industrial to 1100 ppmv. The resulting "climate response functions" allow us to distinguish the impacts of changing greenhouse gasses from climate variability.

5.2. Control Model Dependence on Mixing Nutrients, Oxygen, and Alkalinity

We begin by analyzing uncertainties in A_{Redi} that are reflected the annual-mean steady-state of biogeochemically important fields. Macronutrients (PO_4, Fig 1a) display larger concentrations in the Southern Ocean, which can be attributed to iron limitation. The Southern Ocean is also known as a High Nitrate Low Chlorophyll (HNLC) region in which surface macronutrients are stripped out, even where supply rates are high due to iron limitation, which can also be seen in Fig. 1n (Galbraith et al., 2010). Iron deficiency has been shown to reduce the chlorophyll to carbon ratio, θ, due to chlorophyll synthesis requiring iron (Greene et al., 1991; Sunda and Hunstman, 1997; Marchetti and Harrison, 2007). This is because iron limitation reduces the maximum achievable photosynthetic rate. As a result, when the utility of photons decrease under Fe limitation, light availability becomes a less important limiting factor (Galbraith et al., 2010). Therefore, iron limitation will be most important under low light, and at high temperatures. Iron availability was also found to affect vertical distribution of phytoplankton within the water column and changes in the seasonal cycle of primary production (Galbraith et al., 2010). As seen in Fig. 1b, there are significantly higher values of iron in the subtropics and northern latitudes (with particularly high values in the North Atlantic). Due to the high reactivity and rapid removal of iron from the surface of the ocean via plankton and photochemical breakdown of ligands (Barbeau et al., 2001), the

lifetime of iron is much shorter than that of phosphate or nitrate (Galbraith et al., 2010). This creates a concentration of iron in the North Atlantic, where dust delivery is particularly high. In general, each of the parameterized runs agrees relatively well with observations, with the exception of iron (where we do not have a good global dataset to compare against), giving certainty that our model is credible.

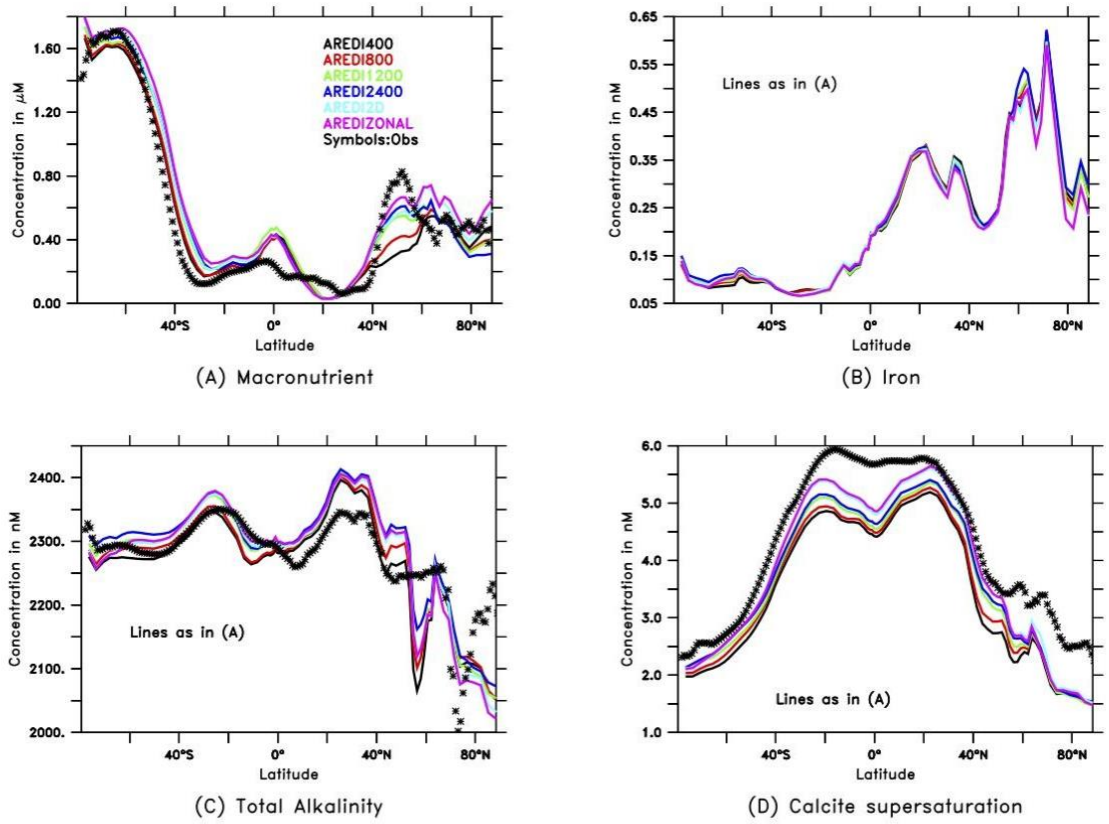

Fig. 1. Global mean state response at surface with six different A_{Redi} parameterizations, compared to observations (symbol). Panels (A) Macronutrient, and (B) Iron (Fe), show differences between observations and the mean experiments. Panels (C) Alkalinity, (D) Calcite (CaCO3) supersaturation represents the efficiency of the model in the mean state presenting results that are nearly identical to observations. Iron observations are not included due to a lack of reliable data.

The degree to which the models agree with one another in Fig. 1 results in a small difference in spread. As stated above, this increases our model's credibility as each of the parameterizations agree well with one another. However, the Northern Hemisphere (NH) appears to be a source where the models disagree both with each other and with observations. Part of the difference in our models compared to observations is due to excessive production within the weakly stratified North Pacific waters to the east of Japan. Within this highly convection region, all the models appear to underestimate surface macronutrient, shown in Fig. 1A, and total Alk, shown in Fig. 1C, compared to observations. The largest underestimate is found in the AREDI400 while ABERZONAL produces macronutrient surface estimates closest to observations, shown in Fig. 1A. This is important to note when analyzing changes in the NH throughout our study, as the spatially dependent models might better produce surface nutrients due to mixing more nutrient across boundary currents.

The value of calcite supersaturation in surface waters is largest in the tropics, with undersaturated waters extending to the poles, as seen in Fig. 1D. In general, the models agree well with another, with the exception of ABERZONAL producing larger concentrations comparatively. Considering observations show larger concentrations of calcite undersaturation throughout the tropics, models that simulate within mixing the boundary currents, such as ABERZONAL, may be more advantageous compared to other models.

The distribution of biota in the interior ocean is strongly dependent on hydrographic parameters. The first of these parameters is hypoxia (oxygen concentration > 2ml/l or 88 μM), where respiration-driven oxygen consumption exceeds the rate at which oxygen is replenished (Gobler & Baumann, 2016). Hypoxia is a complex ecological phenomenon that occurs due to a convergence of factors like nutrient runoff, stratification within the water column, and increased global temperature. The harmful impacts are especially common among surface waters and coastal ecosystems due to eutrophication, leading to the excessive production of organic matter that increases the oxygen demand of coastal ecosystems. Poorly

mixed waters result in trapped oxygen or nutrients in the surface layer as stratification is imposed. The results of oxygen-poor regions greatly inhibit stress on phytoplankton physiology by controlling their metabolic rates, growth rates, and reproduction (Vaquer-Sunyer & Duarte, 2008). As global temperature increase, the respiratory oxygen demand of organisms increases. But, because of climate change, oxygen solubility has decreased. This has ultimately resulted in over 400 identified hypoxic zones in coastal areas (Vaquer-Sunyer & Duarte, 2008). The impacts of disturbing the phytoplankton community, which regulate the quality and quantity of primary production, is eventually transferred up the food web (Basu & Mackey, 2018). Therefore, the growing presence of hypoxic zones may completely restructure trophic efficiency, causing great consequence for marine food webs, and the carbon transferred between species (Basu & Mackey, 2018).

Additionally, the biogeochemical environment is also affected by calcite saturation state, which is a function of temperature, salinity, and pressure (Zeebe and Wolf-Gladrow, 2001). The same nutrient-enhanced respiration of organic matter that creates hypoxic zones also produces high level of CO_2 , leading to low pH and low carbonate ion availability. Calcifying organisms, such as foraminifera, coccolithophores, crustaceans, echinoderms, and molluscs, form their shells and skeletons via the process of calcification. An organism will calcify depending on the amount of carbonate ions, and its biogenic minerals (aragonite and calcite) in the seawater, which is dependent on the saturation state. The saturation state, the thermodynamic potential for a mineral to dissolve, can either be supersaturated or undersaturated with respect to $CaCO_3$. Based on a study done by Berelson et al. (2007), the carbonate system's steady state is achieved when the amount of carbonate produced in the surface water is equal to or exceeding the amount that is exported. When the saturation state ($\Omega CaCO_3$) is equal or greater than 1, then $CaCO_3$ precipitation is favored (Bach, 2015). Regional differences are especially important in this regard because carbonate solubility increases as the temperature decreases, pulling our attention towards the high latitudes.

Given that the models show relatively small differences in surface concentrations of biologically active tracers, one might expect that interior differences would also be smaller. This is not the case. As seen in Fig. 2a, which looks at calcite undersaturation and hypoxia within the water column, both fields are strongly affected by the value of A_{Redi}. As seen in Fig. 2A and B, observations taken from GLODAP show that the N. Pacific deep ocean is largely undersaturated and hypoxic in deeper waters north of the equator. The large-scale structure of calcite undersaturation is to be expected as the upper layers of the ocean, as these areas are generally supersaturated with respect to both mineral phases of $CaCO_3$, whereas the deep waters are largely undersaturated (Sarmiento and Gruber, 2006). This is most extreme in the North Pacific, where the oldest deep waters with the largest accumulation of acidic remineralized carbon are found.

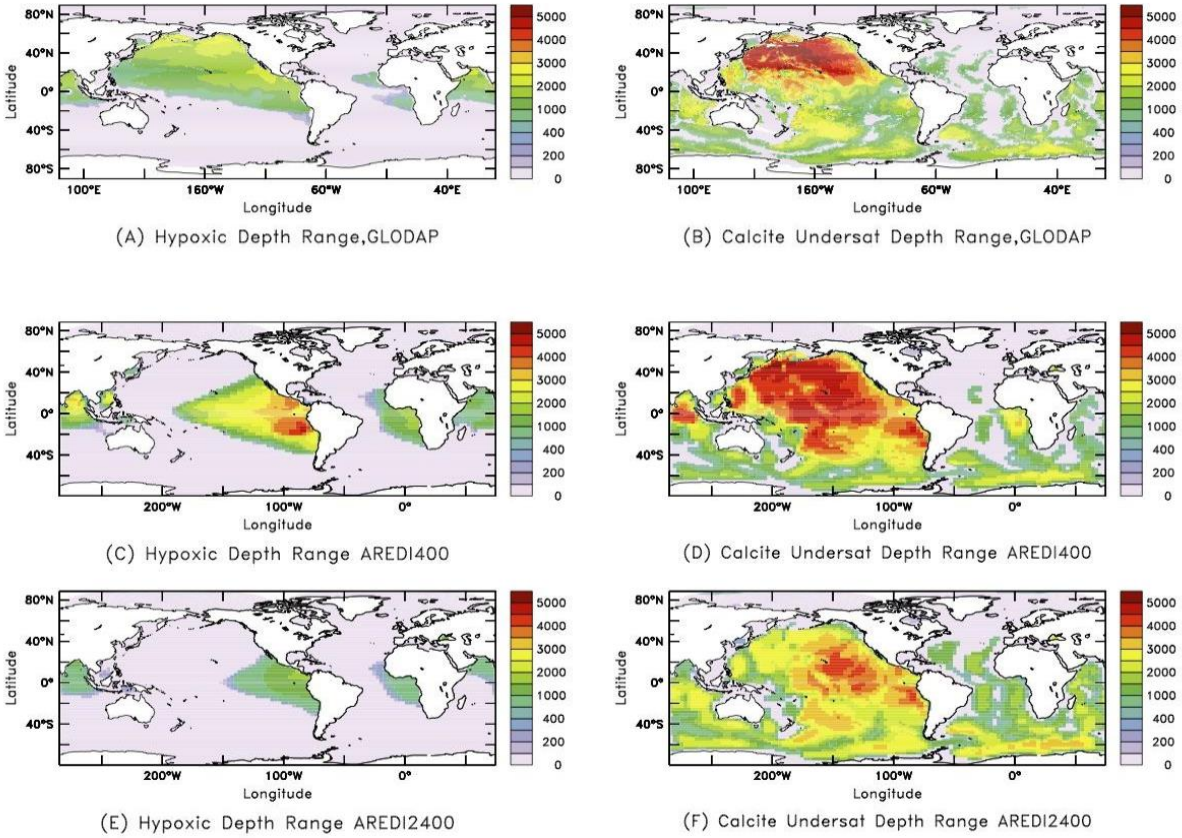

(A) Hypoxic Depth Range,GLODAP

(B) Calcite Undersat Depth Range,GLODAP

(C) Hypoxic Depth Range AREDI400

(D) Calcite Undersat Depth Range AREDI400

(E) Hypoxic Depth Range AREDI2400

(F) Calcite Undersat Depth Range AREDI2400

Fig. 2. Influence of mixing coefficient on mean-state hypoxia and calcite undersaturation. (A) Observations, taken from GLODAP, of global hypoxia, in um, at depth and (B) observations of global calcite undersaturation at depth. (C) Global hypoxic volume and depth range in the mean state and (D) global calcite undersaturation volume and depth range, both with low-mixing model, AREDI400. (E) and (F) compare the same global calcite undersaturation volume and depth range in the mean state, but with high-mixing model, AREDI2400. The unsaturated zone expands by 70 million cubic kilometers from AREDI2400 to AREDI400 an increase of 14%. The 400 case shows largest drop in CO3 saturation in Pacific.

When observing differences in hypoxia between low and high mixing cases, we see a larger volume in the low-mixing case (AREDI400), Fig. 2C. Hypoxic depth ranges up to 4500 m are found, occupying most of the Eastern Pacific, as well as a second intense center in the Bay of Bengal. By contrast, the high-mixing case (AREDI2400) simulates lesser volume and a depth range of 1500m, shown in Fig. 2E. Therefore, as mixing increases, both the range of depth and the horizontal extent of hypoxia shrink. Comparing to observations in Fig. 2A, we can see that neither of the models can properly simulate the hypoxic concentration in the N. Pacific. This is a bias amongst models that is somewhat common (Gnanadesikan et al., 2013).

Similar differences between the low- and high-mixing cases can be seen for calcite undersaturation, as shown in Fig. 2D and 2F. The low-mixing case (AREDI400) results in large volumes of calcite undersaturated waters occupying 584 million cubic kilometers, with depth ranges exceeding 4000 m throughout the Pacific. The AREDI400 case produces more calcite supersaturation in the Atlantic compared to both the observations and the high-mixing case. When increasing A_{Redi} to 2400 m^2s^{-1} calcite undersaturation depth range occupies more of the South Atlantic, but the depth range shallows compared to AREDI400 throughout the Pacific. This results in a decline of undersaturated water of 70 million cubic kilometers constituting a ~14% difference between the 2400 and 400 cases. In general, the low-mixing

case produces too large of a signal compared to observations, however the signal produced in the NP lies closer to the observations compared to the high-mixing case.

5.3. Biogeochemical Cycling in the Mean State

How are these hydrographic differences reflected in biogeochemical cycling? Fig. 3 shows differences in biological variables that are associated with the differences in nutrients shown in Fig. 1. Consistent with Fig. 1, the models show broad-scale agreement with the observations although there are significant differences at the regional level. The modeled concentration of Chl, in mg/m^3, captures the observed contrast between upwelling and downwelling regions with broad similarities to observations in the tropics. However, it tends to overestimate the northern subtropics. As macronutrients in this latitude band are typically not overestimated (Fig. 1A), it is possible that these high Chl concentrations reflect a chl:C ratio that is too large, possibly due to too strong a dependence on iron. Further, an explanation for higher macronutrient concentrations can be due to iron-dependent photosynthesis terms that reduce growth rates in HNLC regions.

Fig. 3C and D show the global impact of iron dependencies on primary production and export production. The method used to estimate the ratio of particulate organic carbon (POC) export to primary production (the *pe*-ratio) is discussed in Dunne et al. (2007). Dunne et al. (2007) states that particle export is dominated by the ability to produce particles throughout primary production. The fraction of phytoplankton with high export efficiencies increases with increasing primary productivity, *pe* ratio increase with primary productivity (Dunne et al., 2007). The models all show similar levels of productivity and export as the (relatively uncertain) observations, with peaks in at around 40S on the equator at 40N. Unsurprisingly, the regional differences in iron supply (Fig. 1B) means that zonally integrated primary production in the iron-poor Southern Hemisphere is similar to that in the high northern latitudes despite the area of the Southern Ocean being much bigger. The models all capture the wide band of high primary productivity associated with equatorial upwelling (Fig. 3C). Both modeled primary

production and modeled particle export show prominent maxima in the equatorial and the southern subpolar regions, with a slightly weaker maximum in the southern subpolar regions, paralleling with Dunne et al. (2007).

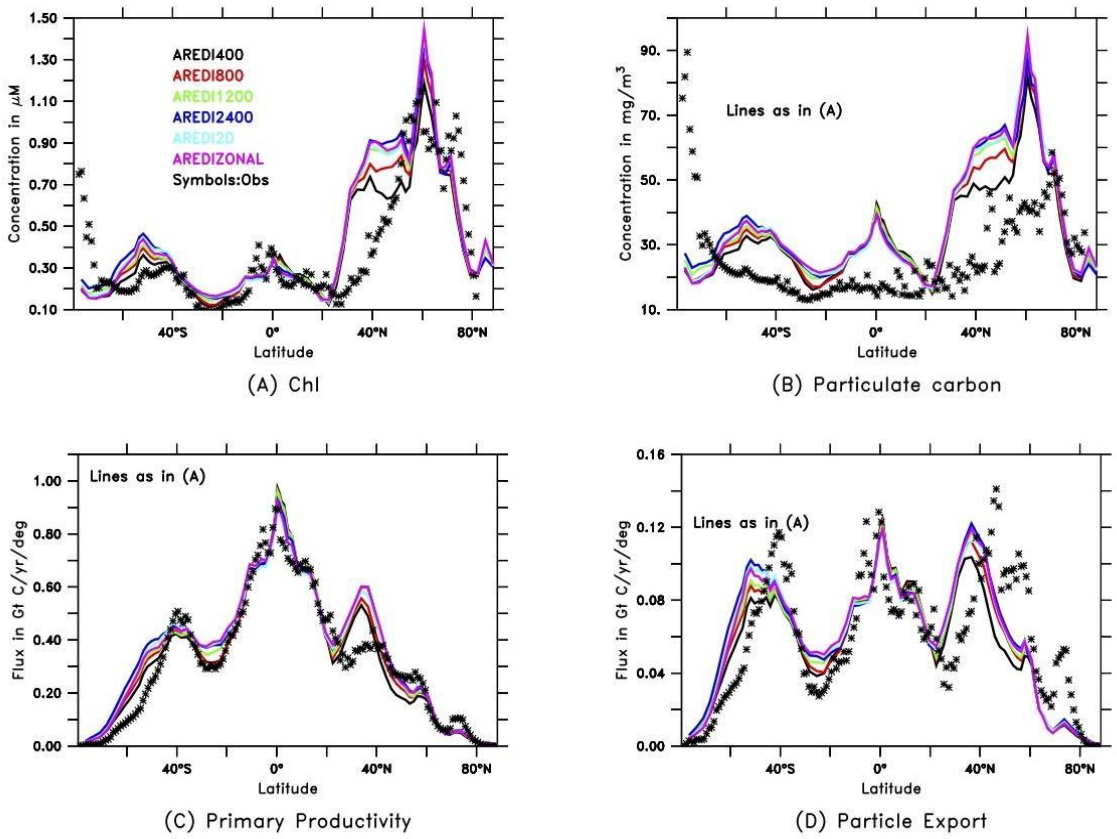

Fig. 3. Comparison between modeled and satellite-based estimates for global chlorophyll, particulate carbon, primary production, and export production run on the full suite of A_{Redi} experiments in the mean state. Panels (C), zonally integrated primary production, and (D) zonally integrated export production, agree well with observations, while panels (A) zonally averaged chlorophyll, and (B), zonally averaged particulate carbon diverge somewhat more from the observations.

6. Results: Model Response to Increased CO_2 (2x and 4x)

6.1. Climate Response

Analyzing the climate response requires us to first examine the magnitude and frequency of sea surface temperatures (SSTs), as well as the change to ice extent under increased CO_2. As shown in Fig. 4, the global response to 572 ppmv of CO_2 on multi-millennial timescales will result in a 0.5-1.0°C increase to SSTs, and an increase of 1100 ppmv CO_2 will result in SSTs increasing by more than 2.5°C. The 2x case shows a gradual response across all models, simulating a similar magnitude of variability in heat content. The consistency of the general shape in Fig. 4A suggests the relationship between the models under the 2x scenario are controlled by the same mechanisms. In contrast, forcing a 4x CO_2 perturbation results in variability between the models, with AREDI400 projecting more of a delayed response compared to AREDI2400 (Fig. 4A). Thomas et al. (2017) notes that while the existence of heat build-up is important for the existence of deep convective events, it is not yet known what mechanism initiates deep convection in the model or sets the timescale for convective variability. Preliminary investigation suggests that many of the differences between the models are due to where and whether convection shuts off. However, this process is nonlinear and may not scale perfectly between different scenarios.

The relatively small differences between models are surprising given the large differences in the initial state. We might, for example, expect that models with more sea ice would have a larger ice-albedo feedback under global warming. Examining the changes in sea ice extent located in the NH (Fig. 4B) has shown that the change in ice extent under quadrupling is about ~2.5 Mkm^2, with only minor dependence on the mixing parameterization used. The sea ice responses are not particularly consistent with the SST responses. For example, the model with a high-mixing parameter, AREDI2400, results in stronger SST warming under quadrupling and more than a 2 Mkm^2 reduction in sea ice cover relative to doubling (Fig. 4B). Whereas running the model with a low-mixing parameter, AREDI400, results in less of a change in SST temperatures but a larger change (~3 Mkm^2) NH sea ice extent. Low-mixing simulations are

characterized by a build-up and subsequent release of abyssal heat in the Southern Ocean, which may explain the strong interdecadal variance we observe compared to high-mixing simulations. On a seasonal scale, the heat fluxes have the biggest impact on buoyancy fluxes, but when examining on a long-term scale we can observe that the freshwater inputs from melting sea ice plays a dominant role in the net extraction of buoyancy in the NH (Gnanadesikan et al., 2012). Lastly, we hypothesize that the availability of sea ice melt decreases in the future, giving reason for less of a change between the perturbations.

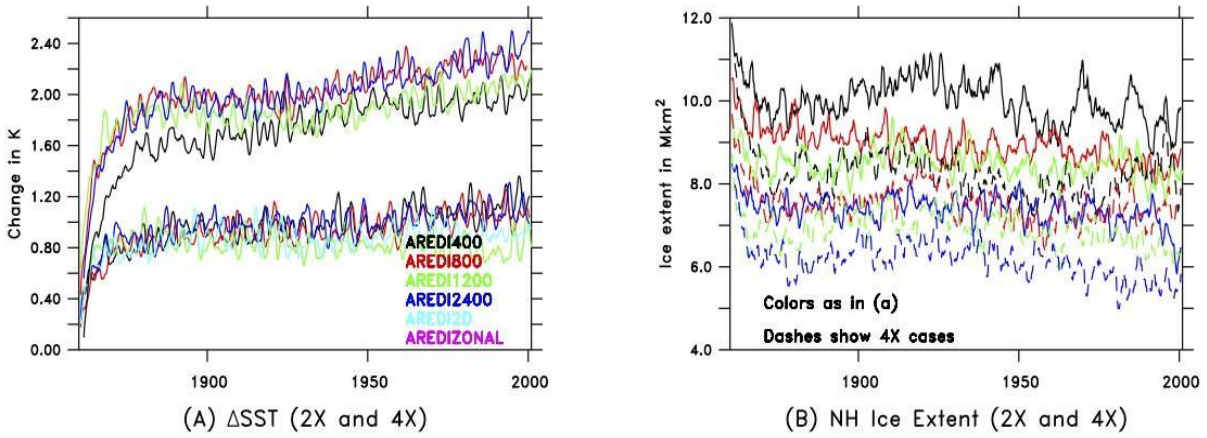

Fig. 4. Time-series run with all six A_{Redi} parameters, including perturbations of 2x CO_2 and 4x CO_2. (A) SST from 1900-1999 for the top five boxes of the ocean module (or 50 m). Solid lines denote simulations under 2x CO_2, dashed lines show the same simulations under 4x CO_2. (B) Sea ice extent in the Northern Hemisphere run with the same simulations as (A).

6.2. Biological Response

Fig. 5 shows a time series of globally integrated relevant variables to biogeochemical cycling and their changes across the different simulations. Fig. 5A shows that Chl is expected to decrease by ~-4-8% under doubling and by 12-16% under quadrupling. The changes do not appear to be monotonic, with the AREDI800 case showing the largest drop under doubling and AREDI800 and AREDI1200 showing the

largest drops under quadrupling. Surface biomass shows a more robust agreement between models (Fig. 5B) with drops around 8% under doubling 16% under quadrupling. The results show an approximately exponential approach to a new equilibrium over the first 40-60 years. The globally integrated primary production is not as strongly affected as the chlorophyll or biomass, with changes of order 4% under doubling and 8% under quadrupling (Fig. 5C). However, the impact of increasing CO_2 results in steeper declines in "large" phytoplankton throughout the NH, so that the global export, as shown in Fig. 5D drops by 8 and 18% under doubling and quadrupling respectively. Studies have indicated the differential response to ocean warming depends on the phytoplankton physiology by controlling metabolic rates (Basu & Mackey, 2018). Considering this, it appears smaller primary producers may thrive (or at least decline less sharply) in a warmer ocean, giving reason for less of a decline in primary productivity change.

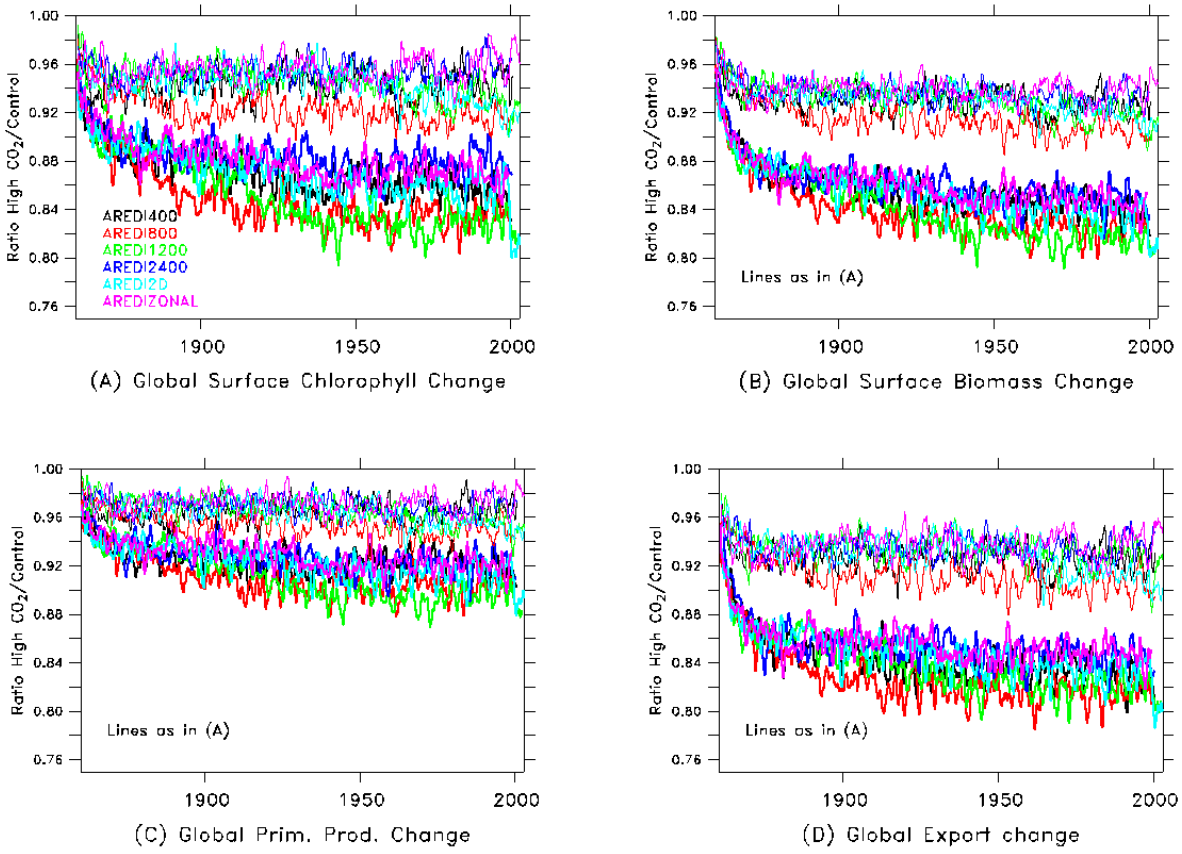

Fig. 5. Changes under doubled and quadrupled CO_2 for the range of A_{Redi} parameters shown as a ratio of high CO_2/control. Solid lines represent the change under 2x perturbations, while the dashed lines represent the change under 4x perturbations. (A) Time-series for the global surface chlorophyll change. (B) Global surface biomass change. (C) Global primary productivity change. (D) Global export change.

We now look at averaged changes from years 1900-2000, after the initial transients in hydrography and biological tracers. As shown in Fig. 6, the model response to increasing CO_2 results in large drops in macronutrient, iron, and Alk in the subpolar NH, consistent with less supply from below. Somewhat surprisingly, increasing CO_2 increases iron in the sub-tropics, presumably because there is less biological removal. The spatial distribution under quadrupling is well correlated with runs that double CO_2. In general, large reductions in concentrations are seen in highly convective regions.

As already noted, the relationship between the mixing coefficient used and the associated biological change is not straightforward. This is likely because of convection. In our control models, higher mixing decreases the stability of polar regions and thus produces more convection in the N Pacific, Southern Ocean, and Atlantic. This allows older waters to surface and provide nutrients to drive productivity. Rising global temperatures have led to a stronger hydrological cycle which acts to reduce this convection, but the stronger the convection is initially, the harder it is to shut off. Therefore, it can be said that convection is already present in our low mixing case (AREDI400), and thus experiences a smaller change under doubling. By contrast, in our high-mixing case (AREDI2400) there is more convection, but it is harder to shut off than in AREDI800 and AREDI1200, giving reason for the biggest changes in phosphate found at intermediate values. However, this is not consistent across all tracers. Fig. 6C demonstrates the largest change in surface Alk in the Northern hemisphere (NH) being associated with the lower mixing cases.

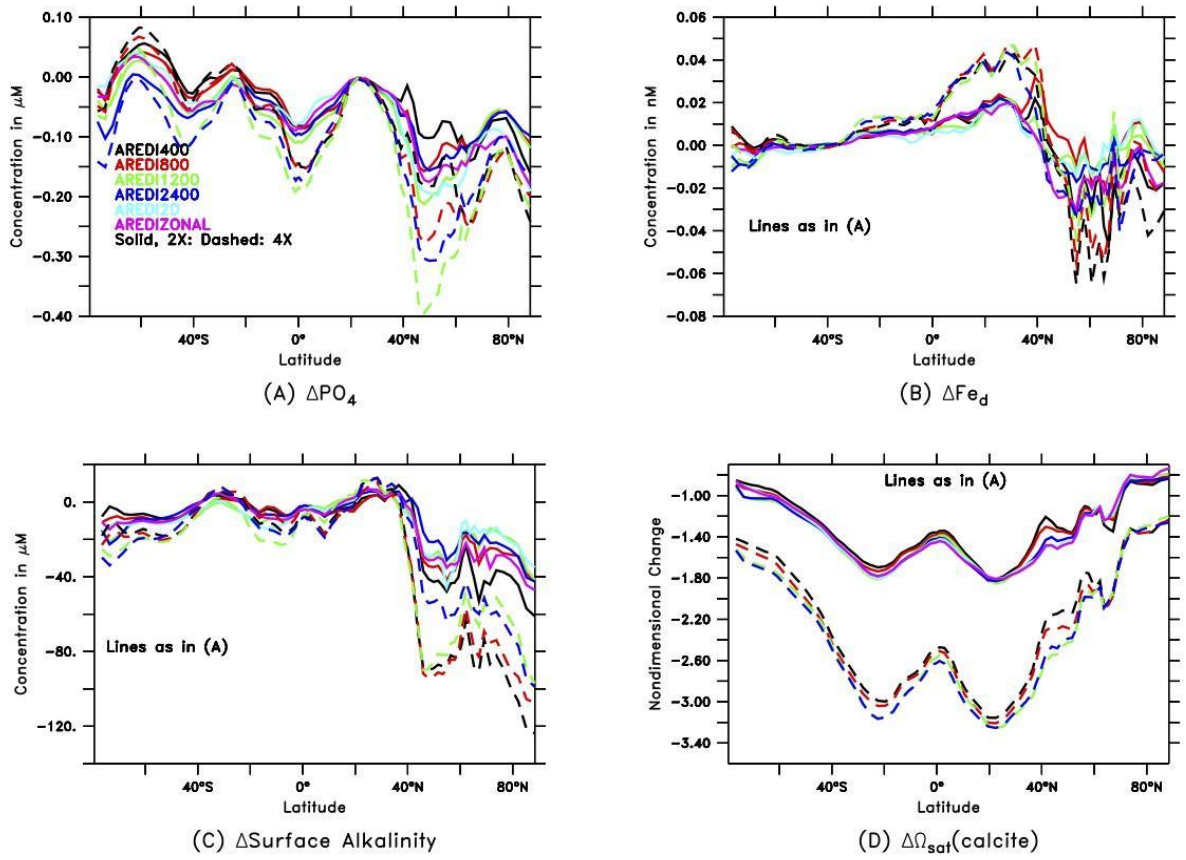

Fig. 6. Changes in chemical concentrations at all depths run with 1860 CO_2 values, except for Alk, which is run at the surface. The solid lines represent model cases parameterized under doubled CO_2; the dashed lines represent changes in models under quadrupled CO_2. (A) Phosphate is used to show changes in macronutrients. (B) Iron shows considerable variability north of the equator, with an increase in AREDI800 under quadrupling. This increase in iron is due to a decrease in phosphate. (C) Surface Alk experiences sharp declines in the North Pacific in ABER2D case, and when quadrupling. More realistic for nutrients, less realistic in terms of alkalinity because of convection. (D) The model response when quadrupling calcite results in Calcite is undersaturated.

6.3. Biological Responses to Climate Change

The changes to biological tracers are much more intense in Fig. 7 compared to chemical tracers in Fig. 6. The northern latitudes show large reductions in Chl, particulate carbon, primary productivity, and particle export when the coefficient is parameterized to anything larger than 400 m^2s^{-1}. AREDI800 appears to be the "tipping point" in regards to physical fluxes, as this is where the convection in the model appears to be most unstable to hydrological perturbations. In previous work (Bahl et al., 2018), export production showed stabilization of convection in the NW Pacific when doubling CO_2. An interesting signal in this figure is the large drop in particle export and productivity in the 4X cases for AREDI400. That this case would show the largest relative drop would not be expected from the relatively small hydrographic changes in nutrient seen in Fig. 6. Looking back at Fig. 1, however, we see that the average zonally-averaged macronutrient concentrations in these latitudes are ~0.4 μM in AREDI400 vs. 0.7 μM in AREDI2400. A drop of 0.25 mM under quadrupling moves this region into being limited by macronutrient, whereas the larger drop in the mixing cases still leaves the macronutrient concentration well above the half-saturation coefficient of 0.1 μM.

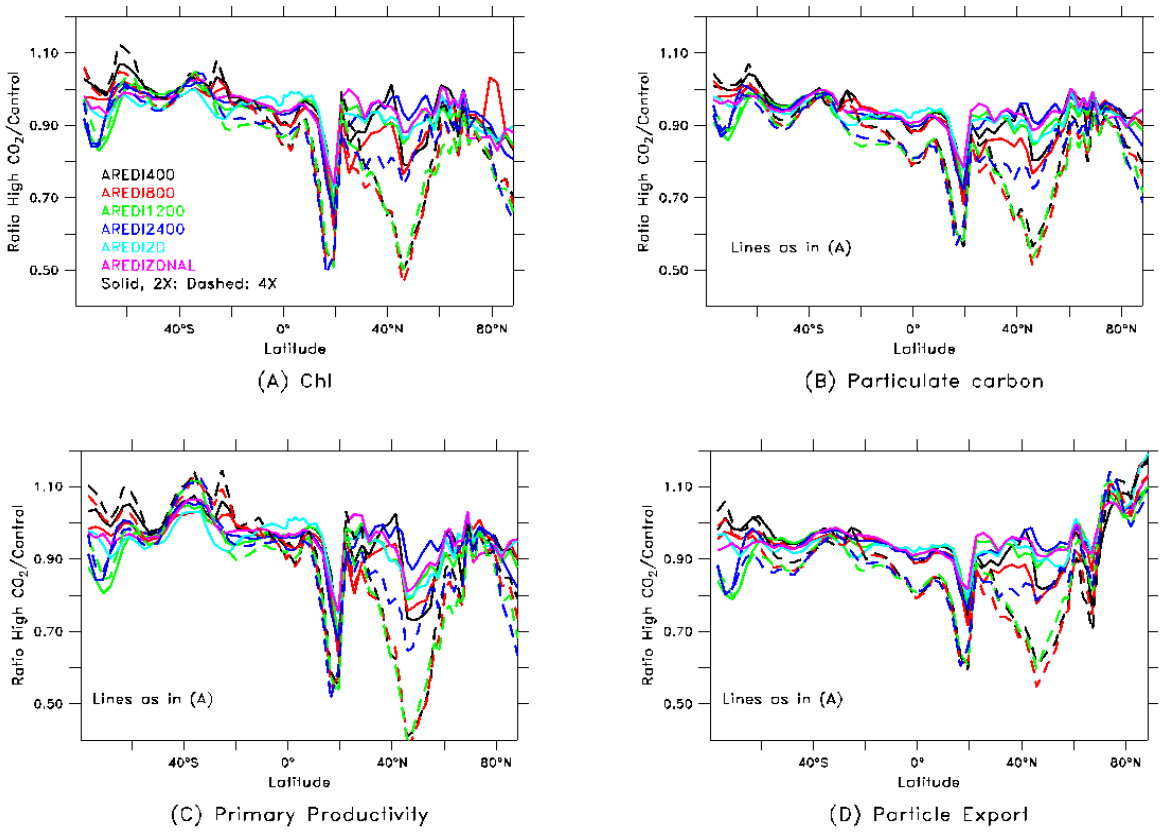

Fig. 7. The tracers run here are the same as those in Fig. 3, with the exception of measuring the ratio of high CO2:control. (A) Chlorophyll experiences a higher amount in 4x run due to higher radiation in the model (92%), while the 2x case lies on the same line, denoting a linear change in Chl and radiation. (B) Particulate carbon decreases under both the 2x and 4x cases, showing considerable variability in the N. Pacific. (C) Primary productivity also declines under increased CO_2 in the N. Pacific. In the first 100 years after quadrupling, biomass drops 16%, which can be attributed to lower rates of Chl and iron depletion. (D) Particle export, 4x case - to first order, the relationship between chlorophyll and export shows the same change. Within the first years under 4x, export drops 8%, the long-term response levels out and eventually drops ~ 20%.

The regional variability regarding Chl is important to note. The Southern Ocean (SO) is described as the largest high nutrient, low chlorophyll (HNCL) province in the world, hence its high abundance of phytoplankton (Deppeler and Davidson, 2017). Iron and silicate are the key nutrients constraining phytoplankton growth in the Sub-Antarctic Zone (SAZ), despite inputs from dust, shelf sediments, and hydrothermal vents (Deppeler and Davidson, 2017; Boyd et al., 2004; Blain et al., 2007; Cassar et al., 2007; Pollard et al., 2009; Boyd and Ellwood, 2010; Tagliabue et al., 2010). However, because iron does not show a decrease throughout each of the models in the SO (Fig. 7B), the difference in volume of phytoplankton biomass between running a low-mixing model and a high-mixing model must be influenced by light availability. These fluxes will be described in section 6.5.

It is common for the SAZ to experience cloudiness and deep mixing. Phytoplankton biomass increases in the high NH because of reduced sea ice cover and a longer growing season, in agreement with earlier findings by Bopp et al. (2001). Further, Fig. 7B shows that running AREDI400 results in large phytoplankton biomass increases under 4x CO_2 in the SO, suggesting that large taxa contribute to a high proportion of carbon export. The same can be said of the NP gyre, where large phytoplankton biomass decreases upwards of 90%. The particle export also decreases in this region under low-mixing (Fig. 7D), informing us that large phytoplankton (characterized as contribution to export production more than small phytoplankton) contribute more in HNLC waters, like that in the SO, explaining why we see a decrease in export. These regional changes impacted by reduced mixed layer depths may have profound consequences on nutrient supply and ocean uptake.

6.4. Changes to Phytoplankton Biomass

We now turn to the regional response of ecosystems to increasing anthropogenic carbon dioxide. The impact of climate change on phytoplankton biomass and community structure involves multiple complex interactions and feedbacks that will likely affect temperature, stratification, and changes to nutrient supply (Chust et al., 2014; Rykaczewski & Dunne, 2010; Taucher & Oschlies, 2011). Changes in total

phytoplankton biomass and large phytoplankton biomass strongly depend on the supply of nutrients into the euphotic zone, which is controlled by ocean circulation and mixing (Schmittner et al., 2008).

Our results reveal that parameterizing the turbulent diffusion coefficient while quadrupling CO_2 results in large nonlinear differences between low and high mixing cases. For instance, looking at changes in total phytoplankton biomass in Fig. 8A and C, it appears the low-mixing case results in an increase in total phytoplankton biomass in the Arctic, Southeast Atlantic Ocean offshore of the Benguela upwelling, the Gulf of Mexico, parts of the Southern Ocean along the coast of Antarctica, and the Sea of Okhotsk (a marginal sea of the western Pacific resting between the west side of the Kamchatka Peninsula and the east side of Russia.) The high-mixing case responds similarly, the magnitudes of changes in biomass change are smaller compared to the low-mixing case.

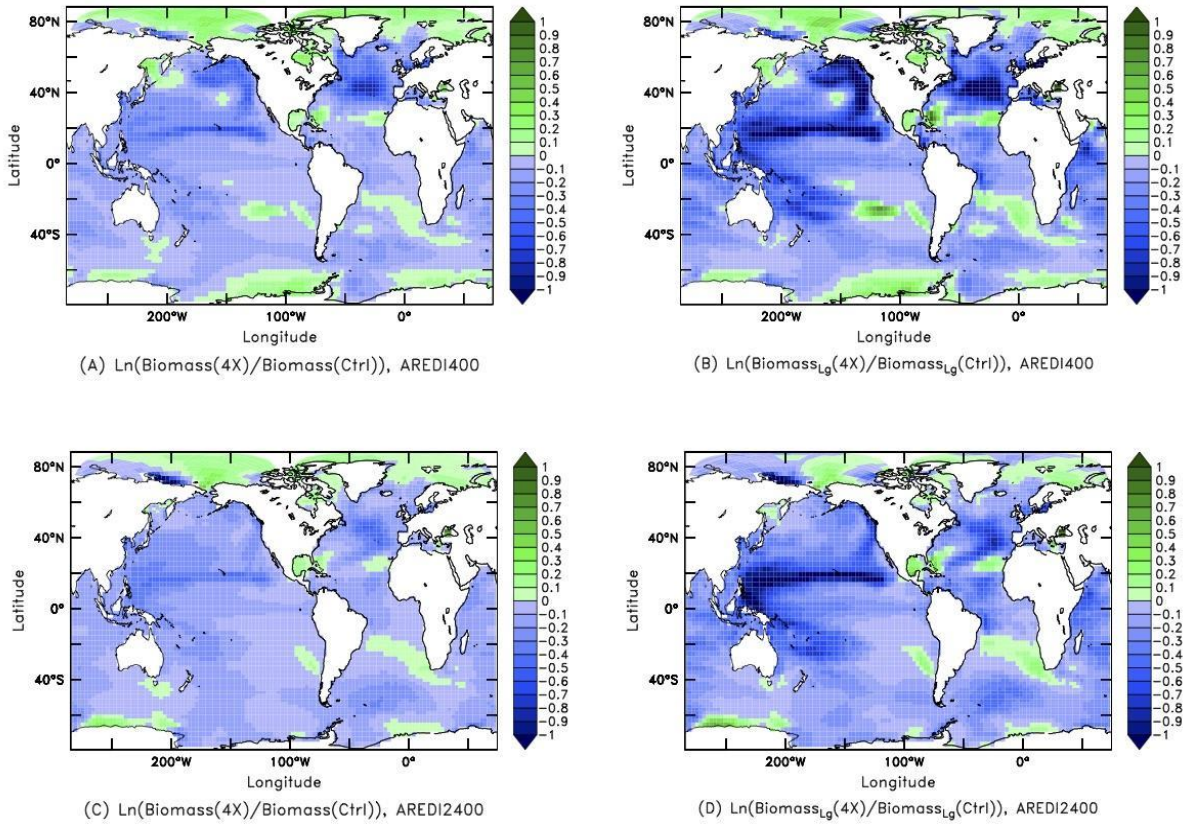

Fig. 8. The first column shows the natural log of global average biomass at all depths parameterized with AREDI400 and AREDI2400 under quadrupled CO2 and the second column is AREDI400 and AREDI2500 quadrupled showing the effects only on large phytoplankton biomass (A) AREDI400 under quadrupled CO2 results in large changes in convective regions, namely the NA and North Pacific. An increase in biomass is show in the Southern Ocean due to a change in iron and light limitation (see Fig. 9) (B) AREDI400 under quadrupling results in large phytoplankton biomass reductions throughout the Northern latitudes, but an increase in the arctic. (C) AREDI2400 4x total biomass occupies less volume increase in Southern Ocean compared to the low-mixing scenario, though general decreases seen throughout all regions with the exception of the arctic. (D) AREDI2400 4x large phytoplankton biomass shows similar changes to AREDI400 with less of an impact in the N. Pacific.

The impact of quadrupling CO_2 is much greater when we focus on the large phytoplankton that form the base of the marine food web. What stands out here are the big declines in biomass in the NH, especially in regards to large phytoplankton biomass. Both the low- and high-mixing models show reductions in large phytoplankton biomass throughout the N. Equatorial current, moving into the Kuroshio current and south into the East Australia Current. The effects can also be seen in the N. Atlantic current. However, the low-mixing model appears to undergo larger reductions in the NA and the NP, whereas the AREDI2400 shows that the regional decreases seen in Fig. 8B are smaller due to greater persistence of deep convection. Regions of high convection thus experience the most extreme declines due to increased precipitation and warming that increases the buoyancy of surface waters, enhancing stratification and reducing mixing layer depths (Deppeler and Davidson, 2017). On the other hand, Fig. 8B shows some increases in large phytoplankton biomass that can be seen in the Sea of Okhotsk, Benguela current mixing into the Brazil current, the Gulf stream propagating into the N. Equatorial current in the Atlantic, along the coast of Antarctica, as well as an interesting increase in the center of the N. Pacific gyre. Thus, parameterizing the model with a low-mixing coefficient results in regional differences simulating upwards of a 60% reduction in large phytoplankton biomass, compared to parameterizing with a high-mixing model that results in a lesser reduction of 45%.

The Southern Benguela Upwelling System (SBUS), located off southwest Africa, had an interesting response when increased CO_2 was detected. Total biomass and large phytoplankton are projected to grow in volume (+0.1-0.4%) shown in Fig. 8, but Fig. 8 projects low light and low nutrient in the SBUS, drawing question on the driver of volume growth. AREDI400 typically limits nutrient availability and light limitation in deeply mixed waters, however SBUS appears to respond differently (Deppeler and Davidson, 2017). This region is an area of high productivity via upwelling and coastal currents, which inherently makes it sensitive to the precise structure of wind stress near the coast (Small et al., 2015). Fig. 7B shows a larger change to this area compared to running AREDI2400 (Fig. 7D). Lower mixing

simulations causes the model to oscillate between convective and non-convective periods (Thomas et al., 2017), which can be hypothesized to force the strong winds offshore, associated with a wind weakening towards the coast that leads to Ekman pumping-driven upwelling (Small et al., 2015).

6.5. Mechanisms Driving Changes in Biomass

By construction, the changes in the biomass in the BLING model reflect changes in growth rate. As described in Dunne et al. (2005), these changes are, again by construction, much greater in large phytoplankton than in small phytoplankton. This size-based relationship results from differential grazing of small and large phytoplankton; as growth rates increase, small phytoplankton concentration increases linearly, while large phytoplankton concentrations increase as the cube of the growth rate. The result is that small phytoplankton are much less sensitive to climate change than large phytoplankton. Our model cannot reproduce past studies that have shown an increased abundance of small phytoplankton species, such as small flagellates (Davidson et al., 2016; Thomson et al., 2016) coincident with a decrease of large phytoplankton. Therefore, the nonlinear relationship between mixing schemes and taxonomic shifts in phytoplankton species contains a number of uncertainties.

Amongst the mechanisms driving changes in biomass is light and nutrient limitation, discussed in Fig. 9. As we can see, higher nutrients and higher light is seen throughout the southern hemisphere in both quadrupling cases. However, AREDI400 reduces light limitation throughout the South Atlantic, counteracting any biomass growth, as seen in Fig. 9. Running the AREDI2400 under quadrupled CO_2 also shows less light limitation in the northern latitudes, especially so in the North Pacific. Under quadrupled CO_2, there is less light and more nutrient limitation in the upper layers of the water column due to reduced diffusion and convection (Fig. 9C and D). However, the impact of CO_2 is easily seen as the melting ice has caused a change in albedo in the Arctic, allowing for higher light absorption. It is interesting that we see the increase in light availability in AREDI400 under quadrupled CO_2, has shown the continued decline in large phytoplankton biomass even compared to AREDI2400, as shown in Fig. 9B.

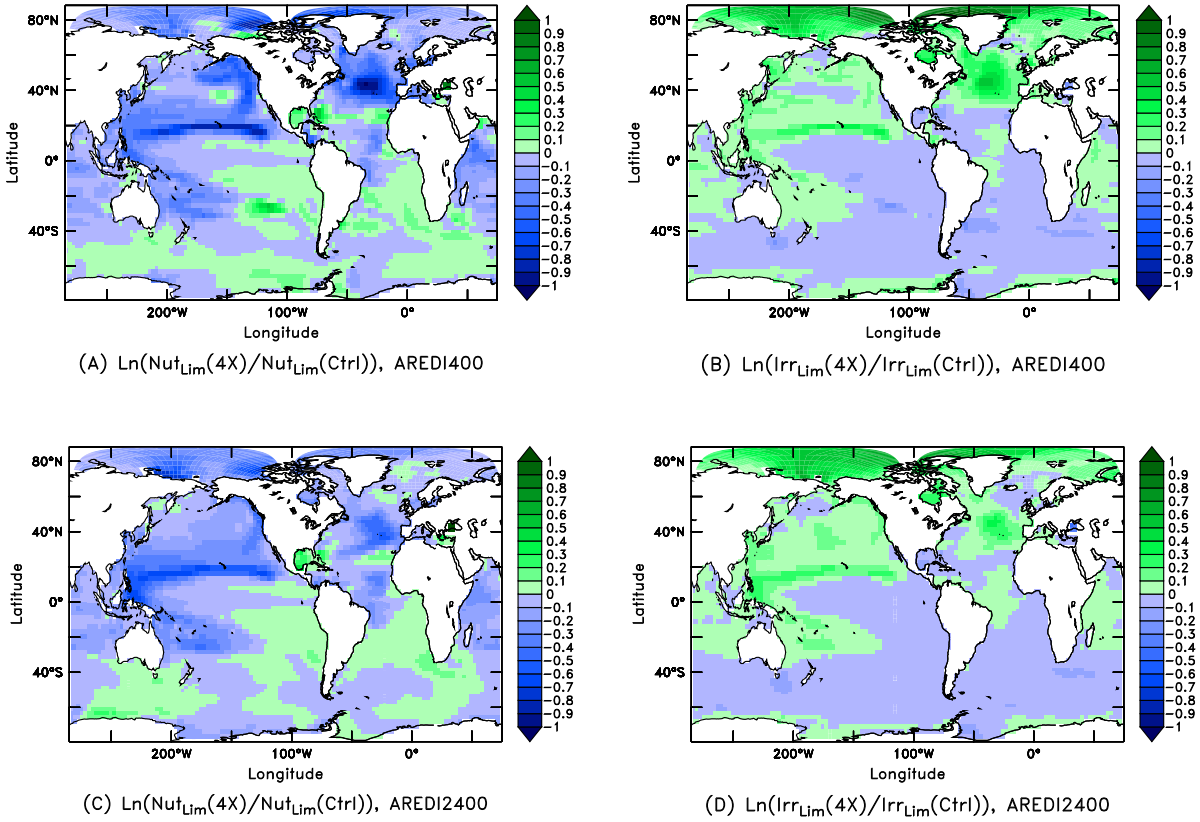

Fig. 9. Change in nutrient and light limitation (Blue denotes lower nutrients, lower light; green denotes higher nutrients, higher light) for the top 50 m under quadrupled CO2. The first column (A, C) shows AREDI400 and AREDI2400 under 4x CO2 measuring nutrient limitation, while the second column (B, D) shows AREDI400 and AREDI2400 under 4x CO2 measuring light limitation. (A) AREDI400 shows large response in northern latitudes, with enhanced nutrient limitation occurring in the NA. (B) The northern latitudes simulated higher light, while the Southern Ocean displays light limitation. (C) High-mixing simulates high nutrients are seen throughout the Southern Hemisphere, but nutrient limitation exists in Northern Hemisphere regions. (D) Lastly, AREDI2400 simulates higher light in the Northern Hemisphere, and lower light throughout the Southern Hemisphere.

In general, both the low- and high-mixing cases show that nutrient limitation would be expected to drive lower growth rates in the NH subtropics but higher growth rates in the equatorial zone and in the Southern Hemisphere. However, the opposite can be said for both cases in regards to light limitation, seen in Fig. 9B and 9D. This means that stronger nutrient limitation is likely responsible for the decrease in phytoplankton biomass in the NP and NA (Fig. 8B and 8D). By contrast, stronger light limitation (which is driven by more cloudiness - not shown) is responsible for the decline in biomass is the Southern Ocean. However, the magnitude of the resulting reduction in primary production, seen in Fig. 5C depends on the mixing parameterization. In the AREDI400 case the reduced input of nutrients in the NP and NA as result of enhanced stratification is much larger in the subpolar gyre than in AREDI2400. In the Arctic, we see an increase in biomass, which is driven by a greater supply of light to the ocean. Therefore, the projections put forth by Chust et al. (2014), which is discussed in the Section 1, parallels well with our study in terms of global declining response in phytoplankton biomass to climate change.

6.6. Change in Saturation State

The degree of calcite saturation is the product of the calcium and carbonate ion concentrations at the *in situ* temperature, salinity, and pressure (Feely et al., 2004). An increase of dissolved CO_2 in the water column leads to a decrease of the CO_3^{2-} ion concentration ($CO_2 + H_2O + CO_3^{2-} \rightarrow 2\ HCO_3^-$), causing a decrease in water pH and a decrease in the saturation state of $CaCO_3$ minerals calcite and aragonite via reduced solubility (Thomas et al., 2017; Hofmann et al., 2009). Calcifying species, such as coccolithophorids (denoted as "large" in our study), foraminifera, and some crustaceans predominantly form calcite from biogenic $CaCO_3$ when building their exo- and endoskeletons (Bach et al., 2015). Upon death, the calcified species fall to the deep ocean while undergoing aggregation, termed "falling snow," and are either deposited in shallow or deep-sea sediments (Feely et al., 2004). The flux of calcite that leaves the surface ocean and arrives at depth to be buried in sediments is only about a third, or ~13% of the surface export (Sarmiento and Gruber, 2006). In contrast to the high burial efficiency of $CaCO_3$, 95% of organic matter is exported from the surface water to be remineralized within the water column, and

only 0.3% of that organic matter export is buried (Sarmiento and Gruber, 2006). This is important to note because the pool of calcite located in the surface sediments, input through riverine weathering, becomes an important part of the global carbon cycle on vast timescales.

The more CO_2 the ocean dissolves, the extent and location of dissolution increases as a function of the decrease in calcite saturation state. As seen in Fig. 10, each simulation shows large calcite undersaturation in the NP. A similar study also found large portions of the NP undersaturated due to increasing anthropogenic CO_2 (Feely et al., 2004). Section 6.4 analyzed and discussed the impacts of changing "large" biomass in the NP, which could be driven by the simulated undersaturation state of AREDI400 (Fig. 10B), thus giving reason for the large changes seen in export production. However, it can also be hypothesized that undersaturated calcite waters are a result of declining biomass. With that being said, very little is known about the molecular uptake of $CaCO_3$ from seawater nor the transfer process to the site of calcification, giving reason for its poorly constrained nature in ESMs.

The NA remains oversaturated, likely due to a lack of accumulation of respired CO_2 in low-mixing cases AREDI400 (Fig. 10B). The Indian Ocean experiences an extreme change, going from supersaturated to undersaturated, when running the AREDI2400 case under 4x perturbations (Fig. 10C and D). The impact of quadrupling CO_2 and then parameterizing with a high-mixing coefficient shows large differences when compared to parameterizing with a low-mixing coefficient. As seen in Fig. 10D, parameterizing with AREDI2400 under 4x perturbations results in 925 Mkm^3 of undersaturated water vs 513 Mkm^3 volume in the control, an 80% increase. By contrast, the AREDI400 case, shows an expansion of 816 Mkm^3 of undersaturated under quadrupling, vs. 584 Mkm^3 in the control. The increase is almost twice as large in the high-mixing. We can see that the AREDI400 model has much smaller changes in the Pacific under doubling, but larger changes in the Southeast Atlantic. The presence of two highly different latitudinal patterns therefore has important implications for ocean acidification research (Bach et al., 2015), further supporting the propagating effects of parameterizing A_{Redi} in an ESM.

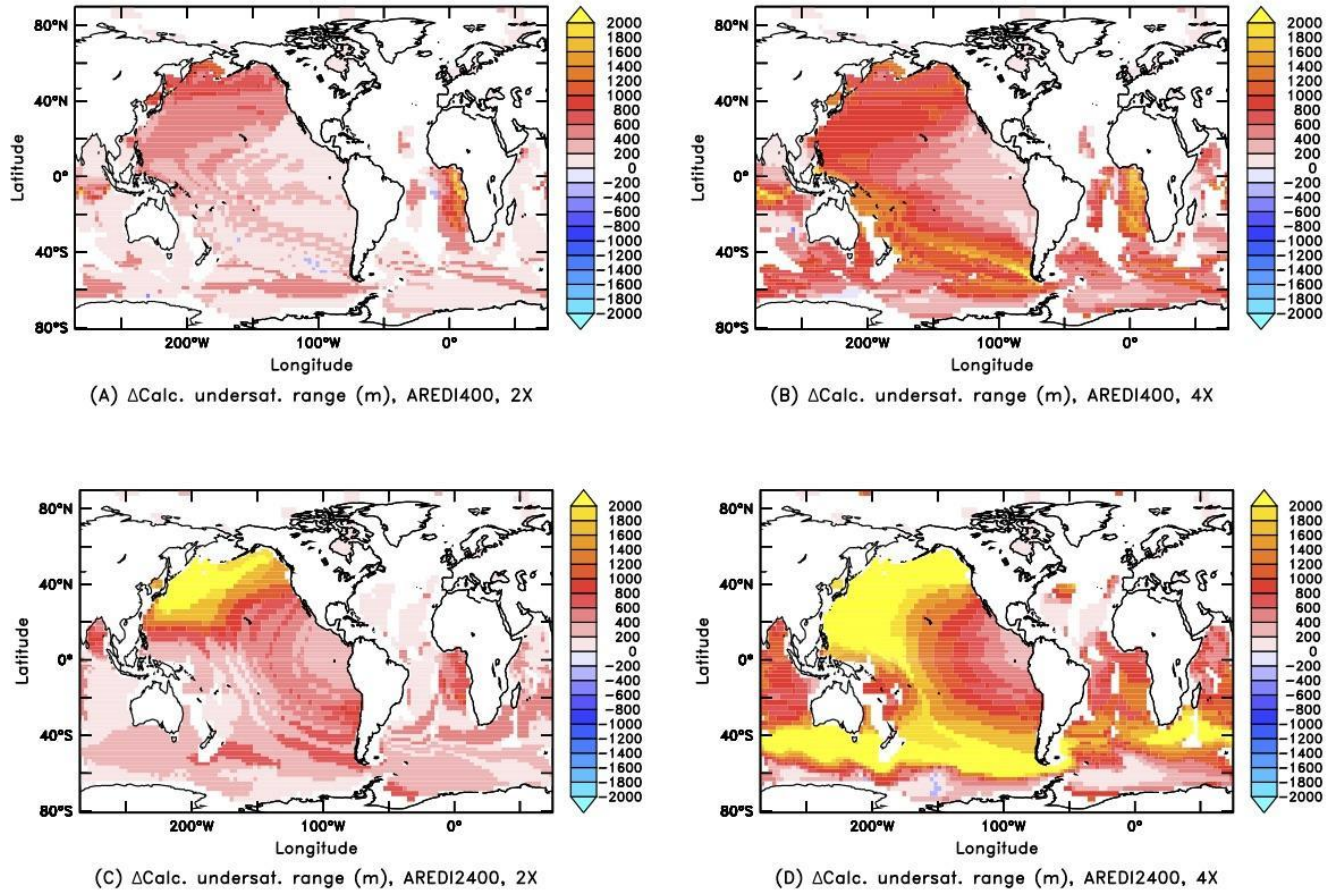

Fig. 10. The volume change of calcite undersaturation at all depths with 2x and 4x CO2 perturbations. (A) AREDI400 under doubled CO2 shows large undersaturation throughout the N. Pacific, and supersaturation in the N. Atlantic. (B) AREDI400 under quadrupled CO2 intensifies undersaturation in the Pacific Ocean and supersaturation in the Atlantic Ocean. In addition, it greatly increases on the boundary currents of Africa, pushing west towards the Indian Ocean. (C) AREDI2400 under doubled CO2 shows similar changes in the N. Pacific, while (D) quadrupled CO2 results in extreme global impacts of undersaturation throughout the Pacific and Southern Ocean.

7. Discussion and Conclusions

Here we present six different parameterizations for the turbulent diffusion, A_{Redi} and their simulated effects on a number of biogeochemical variables, with the corresponding response to doubled and quadrupled CO_2. Based on our analysis, we conclude that the biological response to parameterizing A_{Redi} is nonlinear, however, changes in physical dynamics are shown throughout our study to differ based on the coefficient used. Therefore, determining biogeochemical changes requires constraining the turbulent diffusion coefficient in order to give realistic results. We emphasize that our parameters of choice are not necessarily the correct values to use. We are instead suggesting that the uncertainties simulated throughout the scientific community concerning changes to biological ecosystems under climate change will require further research when tuning an ESM model with physical dynamics. Nonetheless, our results can be used to evaluate the sensitivities and uncertainties in ecosystem response under doubled and quadrupled CO_2.

Parameterizing A_{Redi} carries significant weight in accurately simulating the climate response under anthropogenic climate change. This study has shown the impact of changing the variable affects regional response, biological response, and completely alters physical dynamics, all of which affects sequestration availability. Thus, omitting the variable from ESMs, or failing to parameterize, would likely result in large under or over estimations when calculating the global carbon budget moving into the future. As noted by Gnanadesikan et al. (2018), despite the wide range of A_{Redi} values used in models, very few papers have explored how the value affects model simulations. Additionally, none of the models used in the past round of the IPCC used a parameterization of A_{Redi} that is qualitatively similar to that produced by Koszalka et al. (2009), Abernathey and Marshall (2013), or Cole et al. (2015), the details of which can be read in Gnanadesikan et al. (2018). Based on our results, the impact of using a low-mixing model can result in significant variability in the NP, especially in regards to nutrient fluxes, alk, and primary production.

The combination of wide-ranging temporal and spatial scales associated with biogeochemical feedbacks and fluxes makes the quantitative study of future effects on the oceanic environment a formidable challenge (Werner et al., 2007). For instance, Ollitrault, & de Verdiére, (2002) conducted a float study yielding mixing coefficients of up to 1,900 m^2s^{-1}, while Ledwell et al. (1998) deployed floats in the same area and yielded different estimates due to the presence of large-scale shear, questioning the difference in energetic patches. Simply gathering *in situ* samples for each region across these varying scales is currently not possible, and thus explaining the lack of data in some ESMs. Without data, an initial state for A_{Redi} that accounts for biological and chemical response must be quantified. This has ultimately resulted in models using smaller values of A_{Redi} compared to observations. The variables and interactions require specific time and regional scales due to the complex evolution of mesoscale eddies that by definition, stir and drive fluid particles in a large-scale flow, making it difficult to quantify (Sallée al., 2011).

Our results help explain why long-term changes in biological ecosystem structure is still largely uncertain and even more so its vulnerability to changes in physical dynamics. It is clear that the impact of increasing atmospheric carbon will result in a substantial increase in SSTs, which will cause Arctic sea ice to melt, stabilizing the water column and reducing convection for AMOC and the NP. Phytoplankton biomass appears to decline globally regardless if it is simulated with a high- or low-mixing model, letting us know that physical parameters are less important with 2x CO_2 perturbations. However, parameterizing becomes more important under 4x perturbations within the NP gyre and regional currents, as explained in section 4.4. The importance of understanding future effects is more important than ever. For example, Roxy et al. (2015) observed chlorophyll trends in the Indian Ocean which followed the large-scale trends of sea surface temperatures (SSTs), showing a mean decrease of 20% in marine phytoplankton within the past 6 decades. These findings concluded that tuna catch rates have declined 50-90% in the Indian Ocean during the past five decades, signaling a direct correlation of when phytoplankton also declined (Roxy et

al., 2015). Clearly, research on simulating more realistic results in ESM is needed for fisheries policy, economics, and global trade.

Unfortunately, this growing emphasis requires a demand for observational *in situ* data (for model assimilation), but attaining such observations is difficult when measuring variables that vary in space and time (Brewin et al., 2017). In some cases, regional studies can be done due to a larger amount of *in situ* observations taken from the particular area, however, predicting global changes has been far more difficult, motivating scientists to use satellite-based estimates. For instance, Brewin et al. (2017) ran a study on extensively tested *in situ* data from the NA with an independent satellite dataset to estimate chlorophyll concentration of three phytoplankton classes in a model. The results indicate that dinoflagellate chlorophyll and microplankton chlorophyll increase with SSTs in the NA (Brewin et al., 2017). Deppeler and Davidson (2017) conducted a similar study, but found that long-term trends in primary productivity are not yet detectable due to the large background of interannual/decadal variability and the fact that imposed stressors imposed differ regionally. Both studies state that our understanding of trends is limited by our ability to detect physical changes and thus an enhanced analysis to relieve these uncertainties is needed. In addition, Roxy et al. (2015) analyzed 16 years of quality-controlled blended chlorophyll data and historical simulations using Earth system models that are participating in the Coupled Model Intercomparison Project phase 5 (CMIP5). The observed chlorophyll trends in the Indian Ocean followed the large-scale trends of sea surface temperatures (SSTs), and supported model results showing a mean decrease of 20% in marine phytoplankton within the past six decades (Roxy et al., 2015). These findings are thought to be associated with a reduction of equatorial ventilation in the upper ocean, a slow rate of remineralization in the upper ocean and too large a biologically driven downward flux of particulate organic carbon (Roxy et al., 2015).

Furthermore, while describing the projected effects on specific species is outside the realm of this paper, we find it important to note that a study by Leblanc et al. (2018) encourages the need for increased research determining phytoplankton species classification in a model, as its effects on carbon export are

large, thus effecting the results in our study. The abundant diatom genera species, *Minidiscus*, is often incorrectly classified as "large" in most models and is misidentified and/or systematically under-sampled due to net sizes (Leblanc et al., 2018). The Deep-Water Experiment (DeWex) in 2013 was an intense spring convection event that occurred in the Mediterranean Sea caused by overturning which induced fertilization of the surface waters and triggered phytoplankton blooms, contributing to 15% of the primary production in this area (Leblanc et al., 2018). Interestingly, two of the smallest genus *Minidiscus (*M. *triocalatus* and M. *comicus*) dominated this massive accumulation, while other large diatom species (*Seudo-nitzchia* spp., *Leptocylindrus* spp., *Cylindrotheca* spp., and other large *Thalassiosira* spp.) were observed in elevated concentrations during winter blooms (Leblanc et al., 2018). Thus, the uncertainties surrounding phytoplankton classification in models has first order implications on simulating environmental conditions, especially in regards to export production which impacts the global carbon pump. This is a part of the field that would greatly benefit with improved sampling techniques and research regarding the traits of specific species to properly simulated in ESMs.

Therefore, it can be concluded that constraining the turbulent diffusion coefficient in an ESM is of great importance for not only examining ocean C storage long-term, but also for policymakers to receive more frequent, robust, and transparent data that can be used in part of an NDC pledge or any climate stabilization target. Further, despite this study shedding light on the various uncertainties that show to propagate throughout the model, consensus shows that ESMs are clearly able to simulate natural variability (Maslin et al., 2013). The message of this paper is not to warrant caution when projecting climate change in ESMs, instead it is to unravel the uncertainties to gain a more precise estimation of change induced by anthropogenic carbon. The confidence in ESMs amongst the scientific community was built by the consistency of predictions over decades, and despite the uncertainties, projections have not changed (Maslin et al., 2013). Short term simulations contain the greatest accuracy, and based on the projections, climate change mitigation is more important than ever (Maslin et al., 2013). However, the

complexity of simulating all ecosystem feedbacks on a multi-centennial to millennial timescale has proven itself more difficult and requires increased efforts to support international climate change policy

Future research is needed to best-estimate projections and uncertainty ranges for emissions scenarios. Further, discussed in Gnanadesikan et al. (2015b) it is generally assumed that all passive tracers experience the same value of A_{Redi}, although it is unclear if this is the case for short-lived tracers that have interior sources and sinks, such as the nutrients run in Fig. 1. Research regarding these fluxes would greatly enhance the reliability of an ESM. Lastly, carbon cycle processes and feedbacks, with respect to atmospheric aerosol concentrations, has long been an area of need to simulate numerous natural precursors (Ogunro et al., 2018).

7.1. Policy Implications

On December 12th 2015, the United Nations Convention on Climate Change (UNFCCC) adopted the Paris Agreement, and, as of July 2018, 195 global nations have ratified it. The plan is an important step to mitigate the threats of climate change by holding global temperature below 2°C long-term, with efforts to limit to 1.5°C relative to preindustrial values (Article 2.1(a) of the Paris Agreement). The climate goal was accompanied by an agreement for all nations to submit climate plans in regards to mitigation and adaptation implementation, which is required for re-submission every five years (Rogelj et al., 2017). This Agreement formally defines these plans as Nationally Determined Contributions (NDCs), which can otherwise be characterized as the basic building blocks needed to meet the CO_2 budget assessed by the Intergovernmental Panel on Climate Change (IPCC) in all reports. These numbers are then used by the Global Carbon Project (GCP, http://www.globalcarbonproject.org; Le Quéré et al., 2017). Large uncertainties do still exist among NDC pledges as virtually every aspect was defined at the national level, with little guidance or requirements that would have provided scope, comparability among nations, or quantifications of pledge actions (Rogelj et al., 2017).

Ambiguity has thus resulted in a range of potential GHG emissions predicted for 2030 ranging from 47 - 63 $GtCO_2e\ yr^{-1}$, a ~15-20% variance for 2030 global GHG estimates (Rogelj et al., 2017). Reported in Mengis et al. (2018) the current best estimates of GHG emissions needed to meet the 1.5°C threshold vary widely, from as little as 600 PgC (1 GtC = 1 billion tonnes = 1 x 10^{15}g = 1 Pg) to more than 800 PgC (Mengis et al., 2018). Such large budget imbalances limit the IPCC's ability to verify reported emissions, further exacerbating uncertainties regarding the underlying processes regulating global climate (Le Quéré et al., 2017). This makes it especially difficult to calculate ocean C uptake in Global ocean biogeochemistry models (GOBM) as fossil fuel emission estimates are required to constrain atmospheric measurements of O_2/N_2 to properly simulate "atmospheric potential oxygen," which is needed for understanding air-sea interactions on ocean ecosystems (Ballantyne et al., 2015).

Among the uncertainties concerning quantification and future prediction in regards to the Global Carbon Budget, measurements and emission estimates are still limiting in confidence regarding the calculation of ocean net C uptake (Ballantyne et al., 2015). The 2017 Global Carbon Budget report assessed eight GOBMs constrained by observations for the time period 1959-2016, and concluded a 90% confidence rate, or 1.6 to 2.8 GtC yr^{-1}, of the observed range for the 1990's (Le Quéré et al., 2017). In general, the GOBM ensemble averages a fair combined uncertainty rate of ~ ±0.5 GtC yr^{-1} and a standard deviation of up to ±0.3 GtC yr^{-1} (Le Quéré et al., 2017). However, these uncertainties perpetuate when analyzing on a millennial time-scale and regional differences have proven challenging and more sensitive to change compared to the global whole, as we saw throughout our study. Despite the lack of research on decadal to millennial timescales, a study by Landschützer et al. (2015) offers considerable insight on the significant strengthening of SO uptake, and for the sake of brevity, it concludes that the variability in uptake is quite sensitive to physical climate variability, drawing importance on the A_{Redi} coefficient (Landschützer et al., 2015). Although, it's important to note that the effects of uptake, such as, ocean acidification, eutrophication, de-oxygenation, and a change in saturation state will likely limit its application.

The critical question that emerges from our study is to what extent can the ocean sequester on long time-scales and how are NDCs taking these changes into account? The impact physical dynamics have on ocean storage continues to get peripheral attention in regards to global climate research and climate change policy, further allowing countries to erroneously pledge their NDCs with the intention that ocean sequestration will continue its current rate of ~25% CO_2 absorption each year (Hume, 2018). In 2016, Chile submitted a response to the document FCCC/APA/2016/L.3, stating that the IPCC's Fifth Assessment Report indication of the ocean system as a climate regulator must be integrated into the narrative for long-term mitigation, as the severe consequences of increasing anthropogenic carbon already endured by ocean ecosystems - such as ocean acidification, declining phytoplankton biomass, and changes in dynamical mixing - have been undermined by the very objectives of the Convection of the Paris Agreement (UNFCC.chile). While the Convention explicitly recognizes the importance of conserving the ocean in paragraph 4.1d of the Paris Agreement, it does not state how or to what degree nations should consider the ocean within pledged NDCs. Paragraph 4.1d is as follows (UNFCC):

Art. 4.1 d) "Promote sustainable management, and promote and cooperate in the conservation and enhancement, as appropriate, of sinks and reservoirs of all greenhouse gases not controlled by the Montreal Protocol, including biomass, forests and oceans as well as other terrestrial, coastal and marine ecosystems"

In agreeance with Chile's governmental statement, "conserving and enhancing" the ocean is too vague considering the circumstances, therefore, Parties should consider including mitigation and adaptation strategies particularly pertaining to ocean health (UNFCC.chile). In more concrete terms, integrating the ocean in NDCs cannot result in crediting Parties for the chemical absorption of CO_2 that takes place in their jurisdictional waters. I conclude this paper by stating the need for continued research and understanding on the effects of parameterizing physical dynamics in an ESM and its influence on ocean ecosystem structure.

8. Acknowledgements

This work was made possible by the National Oceanic and Atmospheric Administration (NOAA) under grant NA16OAR4310174 and the National Science Foundation Frontiers in Earth Systems Dynamics Program under grant EAR-1135382.

Within these past two years, burgeoning literature and active research has illuminated my understanding of anthropogenic influence on marine environments and has instilled a greater educated response for climate policy reform and ESM understanding. I am especially indebted to my two mentors, Dr. Ananad Gnanadesikan, Morton K. Blaustein Chair and Professor, and Dr. Jerry Burgess, Program Director of the MS Environmental Sciences and Policy and Sr. Lecturer. Dr. Gnanadesikan has continually been supportive in my research goals as well as influential advisors throughout my academic pursuit and career journey. He provided me an unforgettable experience by teaching me new skills while working as his research assistant, as well as encouraging me to present our work at global conferences. His patience, immense knowledge, and passion for education and research has shown me, by his example, what a good scientist (and mentor) is. Dr. Burgess has encouraged me to push myself in a number of different settings, all the while providing detailed feedback and continued trust. His guidance has been an invaluable part of my time spent at Hopkins and I could not thank him enough for helping me fulfill my educational experience.

Lastly, I would like to thank my friends and family who have provided me extensive personal and professional guidance. Thanks to your love and support, each of you have instilled a greater confidence in the scientist I aspire to be. Finally, I would like to thank all the students, colleagues, and professors that I had the pleasure of working with throughout my degree. Whether I sat by you in a class, analyzed the environment of The Galapagos Islands with you, or conducted research together for a project, I have learned something from each and every one of you and for that I am grateful.

9. References

Abernathey, R. P., & Marshall, J. (2013). Global surface eddy diffusivities derived from satellite altimetry. *Journal of Geophysical Research: Oceans,* 118, 2, 901-916. http://doi.org/10.1002/jgrc.20066

Acevedo-Trejos, E., Brandt, G., Steinacher, M., & Merico, A. (2014). A glimpse into the future composition of marine phytoplankton communities. *Frontiers in Marine Science, 1*(15). doi:10.3389/fmars.2014.00015

Adcroft, A., Hill, C., & Marshall, J. (1997). Representation of topography by shaved cells in a height coordinate ocean model. *Mon. Wea. Rev.,* 125, 2293-2315.

Bach, L. T. (2015). Reconsidering the role of carbonate ion concentration in calcification by marine organisms. *Biogeosciences,* 12, 4939-4951. https://doi.org/10.5194/bg-12-4939-2015

Bahl, A., Gnanadesikan, A., & Pradal, M.-A. (2018). Impact of Parameterized Eddy Mixing on the Sensitivity of Ocean Biogeochemical Cycling to Doubled CO_2 Within an Earth System Model. *Global Biogeochemical Cycles,* in press.

Ballantyne, A. P., Andres, R., Houghton, R., Stocker, B. D., Wanninkhof, R., Anderegg, W., et al., (2015). Audit of the global carbon budget: estimate errors and their impact on uptake uncertainty. *Biogeosciences, 12*, 2565-2584. Doi:10.5194/bg-12-2565-2015

Barbeau, K., Rue, E. L., Bruland, K. W., & Butler, A. (2001). Photochemical cycling of iron in the surface ocean mediated by microbial iron (III) – binding ligands. *Nature,* 413, 409-413.

Basu, S., Mackey K., & R. M. (2018). Phytoplankton as Key Mediators of the Biological Carbon Pump: Their Responses to a Changing Climate. *Sustainability 2018, 10*(3), 869. https://doi.org/10.3390/su10030869

Behrenfeld, M. J., Boss, E., Siegel, D. A., & Shea, D. M. (2005). Carbon-based ocean productivity and phytoplankton physiology from space. *Global Biogeochemical Cycles,* 19, GB1006. doi:10.1029/2004GB002299, 2005

Berelson, W.M., Balch, W.M., Najjar, R., Feely, R.A., Sabine, C., & Lee, K. (2007). Relating estimates of $CaCO_3$ production, export, and dissolution in the water column to measurements of $CaCO_3$ rain into sediment traps and dissolution on the sea floor: A revised global carbonate budget. *Global Biogeochemical Cycles,* 21, GB1024. doi://10.1029/2006GB002803, 2007

Bopp, L., Monfray, P., Aumont, O., Dufresne, J.-L., Le Treut, H., et al. (2001). Potential impact of climate change on marine export production. *Global Biogeochem. Cycles,* 15, 81–99.

Boyd, P. W., McTainsh, G., Sherlock, V., Richardson, K., Nichol, S., Ellwood, M., & Frew, R. (2004). Episodic enhancement of phytoplankton stocks in New Zealand subantarctic waters: contribution of atmospheric and oceanic iron supply. *Global Biogeochem. Cycles,* 18, GB1029. doi:10.1029/2002GB002020, 2004

Boyd, P. W., & Ellwood, M. J. (2010). The biogeochemical cycle of iron in the ocean. *Nat. Geosci.* 3, 675–682. doi:10.1038/NGEO964

Blain, S., Quéguiner, B., Armand, L., Belviso, S., Bombled, B., Bopp, L., et al. (2007). Effect of natural iron fertilization on carbon sequestration in the Southern Ocean. *Nature,* 446, 1070–1074. doi:10.1038/nature05700

Brewin, R. J., Ciavatta, S., Sathyendranath, S., Jackson, T., Tilstone, G., Curran, K. (2017). Uncertainty in Ocean-Color Estimates of Chlorophyll for Phytoplankton Groups. *Front. Mar. Sci, 4*(104). doi: 10.3389/fmars.2017.00104

Cassar, N., Bender, M. L., Barnett, B. A., Fan, S., Moxim, W. J., Levy, H., et al. (2007). The Southern Ocean biological response to Aeolian iron deposition. *Science*, *317*(5841), 1067–1070. doi: 10.1126/science.1144602

Cole, S. T., Wortham, C., Kunze, E., & Owens, B. W. (2015) Eddy stirring and horizontal diffusivity from Argo float observations: Geographic and depth variability. *Geophys. Res. Lett., 42*(10), 3989-3997. http://doi.org/10.1002/2015GL063827

Chust, G., Allen, J. I., Bopp, L., Schrum, C., et al. (2014). Biomass changes and trophic amplification of plankton in a warmer ocean. *Global Change Biology, 20*(7), 2124-2139. doi:10.1111/gcb.12562

Davidson, A., McKinlay, J., Westwood, K., Thomson, P., van den Enden, R., de Salas, M., et al. (2016). Enhanced CO_2 concentrations change the structure of Antarctic marine microbial communities. *Mar. Ecol. Prog. Ser.*, 552, 93–113. doi: 10.3354/meps11742

Delworth, T. L., Broccoli, A. J., Roasti, A., Stouffer, R. J., Balaji, V., Beesley, J. A., Cooke, W. F., et al. (2006). GFDL's CM2 Global Coupled Climate Models. Part I: Formulation and Simulation Characteristics, *J. of Clim. – Special Edition, 19*, 643-674. doi:10.1175/JCLI3629.1

Dengler, A.T. (1985). Relationship between physical and biological processes at an upwelling front off Peru, 15°S. *Deep-Sea Research, 31* (11), 1301-1315. doi:10.1016/0198-0149(85)90050-0

Deppeler, S. L., & Davidson, A. T. (2017). Southern Ocean Phytoplankton in a Changing Climate. *Mari. Sci., 4* (40). doi:10.3389/fmars.2017.00040

DeVries, T., Primeau, F., & Deutsch, C. (2012). The sequestration efficiency of the biological pump. *Geophysical Research Letters*, 39, (L13601). doi:10.1029/2012GL051963

Dunne, J. P., Armstrong, R. A., Gnanadesikan, A., & Sarmiento, J. L. (2005). Empirical and mechanistic models for the particle export ratio. *Global Biogeochemical Cycles*, 19. doi:10.1029/2004GB002390

Dunne, J. P., Sarmiento, J. L., & Gnanadesikan, A. (2007). A synthesis of global particle export from the surface ocean and cycling through the ocean interior and on the seafloor. *Global Biogeochemical Cycles, 21* (4).

Dunne, J.P., John, J. G., Adcroft, A. J., Griffies S. M., Hallberg, R. W., Shevliakova, E., et al. (2012). GFDL's ESM2 Global Coupled Climate–Carbon Earth System Models. Part I: Physical Formulation and Baseline Simulation Characteristics. *Journal of Climate, 25*(19), 6646-6665. http://doi.org/10.1175/jcli-d-11-00560.1

Ducklow, H. W., Steinberg, D. K., & Buesseler, K. O. (2001). Upper Ocean Carbon Export and the Biological Pump. *The Oceanography Society, 14* (4), 50-58.

Eden, C., Jochum, M., & Danabasoglu, G. (2008). Effects of different closures for thickness diffusivity. *Ocean Modelling.*

Feely, R. A., Sabine, C. L., Lee, K., Berelson, W., Kleypas, J., Fabry, V. J., et al. (2004). Impact of Anthropogenic CO_2 on the $CaCO_3$ System in the Oceans. *Science, 305* (5682), 362-366. doi:10.1126/Science.1097329

Feely, R. A., Sabine, C. L., Byrne, R. H., Millero, F. J., Dickson, A. G., Wanninkhof, R., Murata, A., et al. (2012). Decadal changes in the aragonite and calcite saturation state of the Pacific Ocean. *Global Biogeochem. Cycles, 26*, GB3001. doi:10.1029/2011GB004157

Flato, G., J. Marotzke, B. Abiodun, P. Braconnot, S.C. Chou, W. Collins, P., et al. (2013). Evaluation of Climate Models. In: *Climate Change 2013: The Physical Science Basis. Contribution of Working Group I to the Fifth Assessment Report of the Intergovernmental Panel on Climate Change* [Stocker, T.F., D. Qin, G.-K. Plattner, M. Tignor, S.K. Allen, J. Boschung, A. Nauels, Y. Xia, V. Bex and P.M. Midgley (eds.)], *Cambridge University Press*, Cambridge, United Kingdom and New York, NY, USA.

Fox-Kemper, B., Ferrari, R., & Hallberg, R. (2008b). Parameterization of mixed layer eddies. Part I: Theory and diagnosis. *Journal of Physical Oceanography, 38* (6), 1145–1165. doi:10.11752F2007JPO3792.1

Fox-Kemper, B., Danabasoglu, G., Ferrari, R., Griffies, S.M., Hallberg, R. W., Holland, M. M., et al. (2010). Parameterization of mixed layer eddies. III: Implementation and impact in global ocean climate simulations. *Elsevier, Ocean Modelling, 39* (2011), 61-78. doi:10.1016/j.ocemod.2010.09.002

Friedlingstein, P., Meinshausen, M., Arora, V. K., Jones, C. D., Anav, A., Liddicoat, S. K., & Knutti, R. (2014). Uncertainties in CMIP5 Climate Projections due to Carbon Cycle Feedbacks. *Journal of Climate*. *27*. doi:10.1175/JCLI-D-12-00579.1

Fox-Kemper, B., Danabasoglu, G., Ferrari, R., Griffies, S.M., Hallberg, R.W., Holland, M.M., et al. (2010). Parameterization of mixed layer eddies. III: Implementation and impact in global ocean climate simulations. *Ocean Modelling. 39* (2011), 61-78. doi:10.1016/j.ocemod.2010.09.002

Galbraith, E.D., Gnanadesikan, A., Dunne, J. P., & Hiscock, M. R. (2010). Regional impacts of iron-light colimitation in a global biogeochemical model. *Biogeosciences, 7*, 1043-1064. doi:10.5194/bgd-6-7517-2009

Galbraith, E. D., Kwon, E. Y., Gnanadesikan, A., Rodgers, K. B., Griffies, S. M., Bianchi, D., et al. (2011). Climate Variability and Radiocarbon in the CM2Mc Earth System Model. *Journal of Climate, 24*, 4230-4254. doi:10.1175/2011JCLI3919.1

Galbraith, E. D., Dunne, J. P., Gnanadesikan, A., Slater, R. D., Sarmiento, J. L., Dufour, C. O., et al. (2015). Complex functionality with minimal computation: Promise and pitfalls of reduced-tracer ocean biogeochemical models. *Journal of Advances in Modeling Earth Systems, 7*, 2012-2028. doi:10.1002/2015MS000463

Geider, R. J., MacIntyre, H. L., & Kana, T. M. (1997). Dynamic model of phytoplankton growth and acclimation: responses of the balanced growth rate and the chlorophyll a: carbon ratio to light, nutrient-limitation and temperature. *Marine Ecology Progress Series, 148* (1), 187-200.

Gent, P. R., & McWilliams, J. C. (1990). Isopycnal mixing in ocean circulation models. *J. Phys. Oceanogr., 20*, 150-155.

Gent P. R., Willebrand, J., McDougall, T. J., & McWilliams, J. C. (1995). Parameterizing Eddy-Induced Tracer Transports in Ocean Circulation Models, *25* (4), 463-474. dx.doi.org.

Gnanadesikan, A., Pradal, M., & Abernathey, R. (2010). Isopycnal mixing by mesoscale eddies significantly impacts oceanic anthropogenic carbon uptake. *Geophysical Research Letters, 42*, 4249-4255. http://doi.org/10.1002/2015gl064100

Gnanadesikan, A., Dunne, J. P., & John, J. (2012). Understanding why the volume of suboxic waters does not increase over centuries of global warming in an Earth System Model. *Biogeosciences, 9*, 1159-1172. doi:10.5194/bg-9-1159-2012

Gnanadesikan, A., Bianchi, D., & Pradal, M.-A. (2013). Critical role for mesoscale eddy diffusion in supplying oxygen to hypoxic ocean waters. *Geophys. Res. Lett., 40*, 5194-5198. doi:10,1002/grl.50998

Gnanadesikan, A., Pradal M.-A. & Abernathey, R. P. (2015a). Exploring the isopycnal mixing and helium-heat paradoxes in a suite of Earth System Models. *Ocean Science, 11*, 591-605. doi:10.5194/os-11-591-2015

Gnanadesikan, A., Pradal M.-A. & Abernathey, R. P. (2015b). Isopycnal mixing significantly impacts ocean anthropogenic carbon uptake. *Geophys. Res. Lett., 42*, 4249-4255. doi: 10.1002/2015GL064100

Gnanadesikan, A., Russell, A., Pradal, M.-A., & Abernathey, R. (2017). Impact of lateral mixing in the ocean on El Nino in a suite of fully coupled climate models. *Journal of Advances in Modeling Earth Systems, 9*, 2493–2513. doi:10.1002/2017MS000917

Gnanadesikan, A., Koszalka, I., & Pradal, M.-A. (2018). Dispersion, Diffusion, and Confusion: Lateral Mixing in the Ocean. *Annu. Rev. Mar. Sci,* doi:10.1146/annurev-marine-121916-063327

Gobler, C. J., & Baumann, H. (2016). Hypoxia and acidification in ocean ecosystems: coupled dynamics and effects on marine life. *Biol. Lett., 12*(5). Doi:10.1098/rsbl.2015.0976

Greene, R. M., Falkowski, P., & Geider, R. J. (1991). Effect of iron limitation on photosynthesis in a marine diatom. *Limnology and Oceanography, 36* (8), 1772-1782. doi:10.4319/lo.1991.36.8.1772

Griffies, S. M., Biastoch, A., Boning, C., Bryan, F., Danabasoglu, G., Chassignet, E. P., et al. (2009). Coordinated Ocean-ice Reference Experiments (COREs). O*cean Modelling, 26* (1-2), 1-46. https://doi.org/10.1016/j.ocemod.2008.08.007

Hain, M. P. & Sigman, D. M. (2014). The Biological Pump in the Past. *Elsevier, 8 (*18), 485-517. doi:10.1016/B978-0-08-095975-7.00618-5

Hartin, C. A., Bond-Lamberty, B., Patel, P., & Mundra, A. (2016). Ocean acidification over the next three centuries using a simple global climate carbon-cycle model: projections and sensitivities. *Biogeosciences, 13*, 4329-4342. doi:10.5194/bg-13-4329-2016

Hofmann, M., & Schellnhuber, H.-J. (2009). Oceanic acidification affects marine carbon pump and triggers extended marine oxygen holes. *PNAS, 106* (9), 3017-3022. doi:10.1073/pnas.0813384106

Honjo, S., Eglinton, T.I., Taylor, C.D., Ulmer, K.M, Sievert, S.M, Bracher, A., et al. (2014). Understanding the role of the biological pump in the global carbon cycle: An imperative for ocean science. *Oceanography* 27(3):10–16. http://dx.doi.org/10.5670/oceanog.2014.78

Hume, D. (2018). Ocean Storage of CO_2. *The Maritime Executive*. Retrieved from https://www.maritime-executive.com/features/ocean-storage-of-co2#gs.1YAeAXU

Concepts, Definitions, and the Diffusion Coefficient. Retrieved from ifh.uni-karlsruhe.de

Ilyina, T., Six, K. D., Segschneider, J., Maier-Reimer, E., Li, H., & Núñez-Riboni, I. (2012). Global ocean biogeochemistry model HAMOCC: Model architecture and performance as component of the MPI-Earth system model in different CMIP5 experimental realizations. *Journal of Advances in Modeling Earth Systems, 5*, 287-315. doi:10.1029/2012MS000178

Jin, X., Gruber, N., Dunne, J. P., Sarmiento, J. L., & Armstrong, R.A. (2006). Diagnosing the contribution of phytoplankton functional groups to the production and export of particulate organic carbon, $CaCO_3$, and opal from global nutrient and alkalinity distributions. *Global Biogeochemical Cycles, 20*, GB2015. doi:10.1029/2005GB002532

Jungclaus, J. H., Fischer, N., Haak, H., Lohmann, K., Marotzke, J., Matei, D., & Mikolajewicz, U. (2005). Characteristics of the ocean simulations in the Max Planck Institute Ocean Model (MPIOM) the ocean component of the MPI-Earth system model. *Journal of Advances in Modeling Earth Systems, 5*, 422-446. doi:10.1002/jame.20023,2013

Koszalka, I., Bracco, A., McWilliams, J. C., & Provenzale, A. (2009). Dynamics of wind-forced coherent anticyclones in the open ocean. *J. Geophys. Res., 114*, CO8011. doi:10.1029/2009JC005388

Kwon, E.Y., Primeau, F., & Sarmiento, J. L. (2009). The impact of remineralization depth on the air–sea carbon balance. *Nat Geosci., 2* (9), 630–635.

Leblanc, K., Queguiner, B., Diaz, F., Cornet, V., Michel-Rodriguez, M., Durrieu de Madron, X., & Bowler, C. (2018). Nanoplanktonic diatoms are globally overlooked but play a role in spring blooms and carbon export. *Nature Communications, 9* (953). doi:10.1038/s41467-018-03376-9

Le Quéré, C., Andrew, R. M., Friedlingstein, P., Sitch, S., Pongratz, J., Manning, A. C., et al. (2018). Global Carbon Budget 2017. *Earth Syst. Sci. Data, 10*, 405-448. https://doi.org/10.5194/essd-10-405-2018

Ledwell, J. R., Watson, A. J., & Law, C. S. (1998). Mixing of a tracer in a pycnocline. *Journal of Geophysical Research, 103*(21),499–2159.

Lin, S.-J. (2004). A "Vertically Lagrangian" Finite-Volume Dynamical Core for Global Model. *Monthly Weather Review, 132*, 2293-2307.

Maslin, M. (2013). Cascading uncertainty in climate change models and its implications for policy. *The Geographical Journal, 179* (3), 264-271. doi:10.1111/j.1475-4959.2012.00494.x

Marchetti, A. & Harrison, P. J. (2007). Coupled Changes in the Cell Morphology and the Elemental (C, N, and Si) Composition of the Pennate Diatom Pseudonitzschia Due to Iron Deficiency. *Limnology and Oceanography, 52* (5), 2270-2284. doi:10.2307/4502375

Ministerio de Relaciones Exteriores, Gobierno de Chile. (2016). *Submission to the relevance of the ocean in the global response to climate change.* Retrieved from

http://www4.unfccc.int/Submissions/Lists/OSPSubmissionUpload/39_279_131200401965740037-Submission%20on%20NDC%20and%20oceans%20Chile.pdf

Nakicenovic, N. & Swart, R. (2000). Special Report on Emissions Scenarios (SRES) – A special Report of Working Group III of the Intergovernmental Panel on Climate Change. *Cambridge University Press.*

Ogunro, O. O., Elliott, S. M., Wingenter, O. W., Deal, C., Fu, W., Collier, N., & Hoffman, F. M. (2018). Evaluating Uncertainties in Marine Biogeochemical Models: Benchmarking Aerosol Precursors. *Atmosphere, 9* (184), doi:10.3390/atmos9050184

Ollitrault, M., & de Verdiére, A. C. (2002). SOFAR Floats Reveal Midlatitude Intermediate North Atlantic General Circulation. Part I: A Lagrangian Descriptive View. *Journal of Physical Oceanography, 32,* 2020-2033.

Pacanowski, R. C. & Gnanadesikan, A. (1998). Transient Response in a Z-Level Ocean Model That Resolves Topography with Partial Cells. *Monthly Weather Review, 126,* 3248-3270. doi:10.1175/1520-0493(1998)126

Parmesan, C. (2006). Biological and Evolutionary Responses to Recent Climate Change. *Annu. Rev. Ecol. Evol. Syst., 37,* 637-639, doi:10.1146/annurev.ecolsys.37.091305.110100.

Pradal, M.-A., & Gnanadesikan, A. (2014). How does the Redi Parameter for mesoscale mixing impact global climate in an Earth System Model? *J. Adv. Model. Earth Syst., 6,* 586-601. doi:10.1002/2013MS000273

Pollard, R. T., Salter, I., Sanders, R. J., Lucas, M. I, Moore, C. M., Mills, R. A., et al. (2009). Southern Ocean deep-water carbon export enhanced by natural iron fertilization. *Nature, 457,* 577–580. doi: 10.1038/nature07716

Prinn, R. G. (2011). Development and application of earth system models. *PNAS, 110* (1), 3673-3680. doi:10.1073/pnas.1107470109

Redi, M. H. (1982). Ocean isopycnal mixing by coordinate rotation. *J. Phys. Oceanogr*. *12*, 1154-58.

Riebesell, U., Kortzinger, A., & Oschlies, A. (2009). Sensitivities of marine carbon fluxes to ocean change. *PNAS, 106* (49), 20602-20609. doi://10.1073/pnas.0813291106

Ridgwell, A., & Zeebe, R.E. (2005). The role of the global carbonate cycle in the regular evolution of the Earth system. *Earth and Planetary Letters, 234* (2005), 299-315.

Rogelj, J., Fricko, O., Meinshausen, M, Krey, V., Zilliacus, J. J. J., & Riahi, K. (2017). Understanding the origin of Paris Agreement emission uncertainties. *Nature communications, 8*(15748). DOI: 10.1038/ncomms15748

Roxy, M. K., Modi, A., Murtugudde, R., Valsala, V., Panickal, S., & Prasanna Kumar, S. (2015). A reduction in marine primary productivity driven by rapid warming over the tropical Indian Ocean. *Geophysical Research Letters, 43* (2), 826-833. doi:10.1002/2015GL066979

Rykaczewski, R. R. & Dunne, J. P. (2010). Enhanced nutrient supply to the California Current Ecosystem with global warming and increased stratification in an earth system model. *Geophysical Research Letters, 37,* L21606. doi:10.1029/2010GL045019

Sallée, J. B., Speer, K., & Rintoul, S. R. (2011). Mean-flow and topographic control on surface eddy-mixing in the Southern Ocean. *Journal of Marine Research, 69* (4-6), 753-777.

Sarmiento, J. L. & Gruber, N. (2006). *Ocean Biogeochemical Dynamics.*

Schmittner, A., Oschlies, A., Giraud, X., Eby, M., & Simmons, H. L. (2005). A global model of the marine ecosystem for long-term simulations: Sensitivity to ocean mixing, buoyancy forcing, particle sinking, and dissolved organic matter cycling. *Global Biogeochemical Cycles, 19,* GB3004. doi:10.1029/2004GB002283

Schmittner, A., Oschlies, A., Matthews, H.D., & Galbraith, E.D. (2008). Future changes in climate, ocean circulation, ecosystems, and biogeochemical cycling simulated for a business-as-usual CO2 emission scenario until year 4000 AD. *Global Biogeochem. Cycles, 22,* GB1013. doi:10.1029/2007/GB002953

Shen, Z., & Ming, Y. (2018). The Influence of Aerosol Absorption on the Extratropical Circulation. *Journal of Climate, 31*(15). Doi:10.1175/JCLI-D-17-0839.1

Sijp, W. P., Bates, M., & England, M. H. (2006). Can isopycnal mixing control the stability of the thermohaline circulation in ocean climate models? *Journal of Climate.* doi:10.1175/JCL3890.1

Simmons, H. L., Jayne, S. R., St. Laurent, L. C., & Weaver, A. J. (2004). Tidally driven mixing in a numerical model of the ocean general circulation. *Ocean Model., 6*, 245-263.

Small, J. R., Curchister, E., Hedstrom, K., Kauffman, B., & Large, W. G. (2015). The Benguela Upwelling System: Quantifying the Sensitivity to Resolution and Coastal Wind Representation in a Global Climate Model*. *Journal of Climate, 28*, 9409-9432. doi:10.1175/JCLI-D-15-0192.1.

Sunda, W. G., & Hunstman, S. A. (1997). Interrelated influence of iron, light and cell size on marine phytoplankton growth. *Nature, 390*, 389-392.

Tagliabue, A., Bopp, L., Dutay, J.-C., Bowie, A. R., Chever, F., Jean-Baptiste, P., et al. (2010). Hydrothermal contribution to the oceanic dissolved iron inventory. *Nat. Geosci., 3*, 252–256. doi: 10.1038/ngeo818

Taucher, J., & Oschlies, A. (2011). Can we predict the direction of marine primary production change under global warming? *Geophysical Research Letters, 38* (2). doi:10.1029/2010GL045934

Thomas, J., Waugh, D., & Gnanadesikan, A. (2017). Relationship between ocean carbon and multi-decadal variability. *J. Climate*. Doi:10.1175/JCLI-D-17-0134.1, in press.

Thomson, P., Davidson, A., & Maher, L. (2016). Increasing CO_2 changes community composition of pico- and nano-sized protists and prokaryotes at a coastal Antarctic site. *Mar. Ecol. Prog. Ser., 554*, 51–69. doi: 10.3354/meps11803

United Nations (2015). *Paris Agreement*. Retrieved from https://unfccc.int/sites/default/files/english_paris_agreement.pdf

Vaquer-Sunyer, R., & Duarte, C. M. (2008). Thresholds of hypoxia for marine biodiversity. *PNAS, 105*(40), 15452-15457. https://doi.org/10.1073/pnas.0803833105

Werner, F. E., Cowen, R. K., & Paris, C. B. (2007). Coupled Biological and Physical Models: Present Capabilities and Necessary Developments for Future Studies of Population Connectivity. *Oceanography, 20* (3), 54-69.

Wootton, J. T., Pfister, C. A., & Forester, J. D. (2008). Dynamic patterns and ecological impacts of declining ocean pH in high-resolution multi-year dataset. *PNAS, 105* (48), 18848-18853. doi:10.1073/pnas.0810079105

Zeebe, R. E. & Wolf-Gladrow, D. (2001). CO2 in Seawater: Equilibrium, Kinetics, Isotopes. *Elsevier Oceanography Series, 65* (1).